NASA TECHNICAL NOTE

NASA TN D-6217

NASA TN D-6217

A SIMPLE INTEGRAL METHOD FOR THE CALCULATION OF REAL-GAS TURBULENT BOUNDARY LAYERS WITH VARIABLE EDGE ENTROPY

by Charles B. Johnson and Lillian R. Boney

Langley Research Center
Hampton, Va. 23365

NATIONAL AERONAUTICS AND SPACE ADMINISTRATION • WASHINGTON, D. C. • JUNE 1971

ERRATA

NASA Technical Note D-6217

A SIMPLE INTEGRAL METHOD FOR THE CALCULATION OF REAL-GAS TURBULENT BOUNDARY LAYERS WITH VARIABLE EDGE ENTROPY

By Charles B. Johnson and Lillian R. Boney

June 1971

Page 23, line 6: Change 223 to 279.

Page 26, line 8: Change 265 to 165 (2 places).

Page 27, lines 1 and 2: Change 265 to 165.

Page 28, line 5 (bottom line): Change 200 to 100.

Page 38, bottom line: Change 250 to 165.

Issued October 1972

Errata inserted
7 Nov 72 JA

NASA-Langley, 1972

1. Report No.	2. Government Accession No.	3. Recipient's Catalog No.
NASA TN D-6217		

4. Title and Subtitle	5. Report Date
A SIMPLE INTEGRAL METHOD FOR THE CALCULATION OF REAL-GAS TURBULENT BOUNDARY LAYERS WITH VARIABLE EDGE ENTROPY	June 1971
	6. Performing Organization Code
7. Author(s)	8. Performing Organization Report No.
Charles B. Johnson and Lillian R. Boney	L-7415
	10. Work Unit No.
9. Performing Organization Name and Address	129-01-20-07
NASA Langley Research Center Hampton, Va. 23365	11. Contract or Grant No.
	13. Type of Report and Period Covered
12. Sponsoring Agency Name and Address	Technical Note
National Aeronautics and Space Administration Washington, D.C. 20546	14. Sponsoring Agency Code

15. Supplementary Notes

16. Abstract

An integral method for computing the turbulent boundary layer is presented. The method includes the effect of equilibrium air chemistry and variable edge entropy. A modified Crocco enthalpy velocity relationship is used for the enthalpy profiles and an empirical correlation of the N-power law profile is used for the velocity profile. The skin-friction-coefficient expressions of Spalding and Chi and Van Driest are used in the solution of the momentum equation and in the heat-transfer predictions that use several modified forms of Reynolds analogy.

Heat-transfer data measured in ground tests on a flat plate at a Mach number of 6.0 and on blunt cones at Mach numbers of 8.0 and 11.5 are in good agreement with predictions based on the present method. Sample calculations showing the effect of variable entropy and nose bluntness are presented for flight calculations at approximately 6.09 km/sec (20 000 ft/sec).

17. Key Words (Suggested by Author(s))	18. Distribution Statement
Calculation of turbulent boundary layers Real gas Variable entropy	Unclassified – Unlimited

19. Security Classif. (of this report)	20. Security Classif. (of this page)	21. No. of Pages	22. Price*
Unclassified	Unclassified	45	$3.00

*For sale by the National Technical Information Service, Springfield, Virginia 22151

A SIMPLE INTEGRAL METHOD FOR THE CALCULATION OF REAL-GAS TURBULENT BOUNDARY LAYERS WITH VARIABLE EDGE ENTROPY

By Charles B. Johnson and Lillian R. Boney
Langley Research Center

SUMMARY

A simple integral method for the calculation of an equilibrium air turbulent boundary layer with variable entropy effects on a blunt axisymmetric body is presented. A modified Crocco enthalpy velocity relationship is used for the enthalpy profiles and an empirical correlation of the N-power law profile is used for the velocity profiles. The skin-friction coefficient expressions of Van Driest and Spalding and Chi, corrected for axisymmetric flow by a turbulent Mangler transformation are used in the solution of the momentum equation. Heat-transfer predictions are obtained by use of various modified forms of Reynolds analogy.

Experimental heat-transfer data from wind-tunnel tests on a flat plate at Mach 6.0 and on blunt 5° half-angle cones at Mach 8.0 and 11.5 are compared with the results of the method and good agreement is obtained. In addition, sample calculations are presented for a 5° half-angle cone at flight conditions of approximately 6.09 km/sec (20 000 ft/sec) at an altitude of 18.29 km (60 000 ft). The calculations show the effect of the variable entropy on the flow properties external to the boundary layer as well as on the boundary-layer integral parameters.

INTRODUCTION

In recent years the ability to predict the properties of compressible turbulent boundary layers has been developed to a significant degree as evidenced by the numerous sophisticated finite-difference methods of solution. A review of most of the compressible turbulent boundary-layer-calculation methods prior to 1967 is given in references 1 to 3 and the significant developments in computation methods since 1967 are given in reference 4. Integral methods have been used to compute the turbulent boundary layer for many years and these methods have some distinct advantages over the more sophisticated finite-difference methods. In some instances, in reference 5, for example, it was found there was no significant gain in accuracy for a particular finite-difference numerical

solution compared with the three less rigorous, but much faster, integral methods. Furthermore, when real-gas and variable-entropy considerations are added to a turbulent-boundary-layer solution, the simplicity of an integral method becomes even more desirable.

This paper presents a simple integral method for computing the compressible turbulent boundary layer with equilibrium air chemistry and variable-entropy edge effects. This paper describes in some detail the method and techniques used in the computer program to make the transitional and turbulent boundary-layer calculations. The method uses velocity and enthalpy profile correlations which are based directly on ground-test experimental data. The calculations are carried out in the physical plane, by using either the Van Driest II (ref. 6) or the Spalding-Chi (ref. 7) skin-friction relations and the Reynolds analogy to obtain heat transfer. The method is applied herein to a blunt axisymmetric body; however, the method has shown good agreement with data for nozzle wall boundary layers over a wide range of conditions. (See ref. 8.)

SYMBOLS

Values are given in both SI and U.S. Customary Units. The measurements and calculations were made in U.S. Customary Units.

A	area
A_R, B_R	coefficients in equations (10) and (12)
a	speed of sound
$\overline{C}_F$	average skin-friction coefficient based on conditions at edge of boundary layer
C_f	local skin-friction coefficient based on conditions at edge of boundary layer
F_c	functions given by equations (20), (21), and (22)
F_{MT}	Mangler transformation factor
g_c	a dimensional constant
H	total enthalpy
h	static enthalpy

$\bar{h}$	heat-transfer coefficient
M	Mach number
N	exponent in velocity-profile relation
N_{Pr}	Prandtl number
N_r	recovery factor
$N_{St,e}$	local Stanton number based on conditions at the edge of the boundary layer
p	pressure
$\bar{q}$	normalized heat-transfer rate
q	heating rate
R	unit Reynolds number
R_{AF}	Reynolds analogy factor
$R_{e,x}$	local Reynolds number based on surface distance x/r_n
$R_{e,\theta}$	local Reynolds number based on momentum thickness
r_b/r_n	dimensionless body radius
r_n	nose radius
r_s/r_n	dimensionless radius out to shock (entering stream tube)
S	entropy
T	temperature
u	velocity along x/r_n
v	velocity along y/r_n

x	surface distance
x/r_n	normalized surface distance from stagnation point or sharp-cone apex
x_{vo}	distance from virtual origin of turbulent boundary layer
y/r_n	normalized coordinate normal to wall
z	correlation parameter defined by equation (8)
α_R	exponent in equation (10)
γ	ratio of specific heats
δ/r_n	dimensionless boundary-layer thickness
δ^*/r_n	dimensionless displacement thickness
θ/r_n	dimensionless momentum thickness
θ_c	cone half-angle
ρ	density
τ	shear stress

Subscripts:

aw	adiabatic wall
e	edge of boundary layer
i	incompressible value
max	maximum
R	one of three regions in boundary layer, I, II, or III
s	shock conditions

t	stagnation conditions
tr	transition
w	wall
∞	free-stream value

Primes denote evaluation at reference enthalpy condition of equations (13).

DESCRIPTION OF THEORY

An integral method for the calculation of the equilibrium air compressible turbulent boundary layer over blunt cones including the effects of variable entropy is presented. The present method has been developed from a revision of the integral method described in reference 9. The new method has also been used extensively for nozzle boundary-layer calculations over a wide range of conditions. Results are compared with data on nozzle walls at Mach numbers of 6, 8, and 19 in reference 8.

Variable-Entropy Momentum Integral Equation

The boundary-layer equations for the conservation of mass and momentum for application to a body of revolution at zero angle of attack are

$$\frac{\partial \rho u \frac{r_b}{r_n}}{\partial \frac{x}{r_n}} + \frac{\partial \rho v \frac{r_b}{r_n}}{\partial \frac{x}{r_n}} = 0 \tag{1}$$

$$\rho u \frac{\partial u}{\partial \frac{x}{r_n}} + \rho v \frac{\partial u}{\partial \frac{y}{r_n}} = - \frac{dp}{d \frac{x}{r_n}} + \frac{\partial \tau}{\partial \frac{y}{r_n}} \tag{2}$$

where $p = p(x)$ and $\frac{\delta}{r_n} << \frac{r_b}{r_n}$.

Equations (1) and (2) are combined and integrated from the wall to the edge of the boundary layer. The resulting equations are cast in an integral form amenable for numerical integration as

$$\frac{d \frac{\theta}{r_n}}{d \frac{x}{r_n}} = \frac{C_f}{2} - \frac{\theta}{r_n}\left[\left(2.0 + \frac{\delta^*/r_n}{\theta/r_n}\right)\frac{1}{u_e}\frac{du_e}{d \frac{x}{r_n}} + \frac{1}{\rho_e}\frac{d\rho_e}{d \frac{x}{r_n}} + \frac{1}{r_b/r_n}\frac{d \frac{r_b}{r_n}}{d \frac{x}{r_n}}\right] + \frac{\delta/r_n}{u_e}\left(\frac{dp_e}{d \frac{x}{r_n}}\frac{g_c}{\rho_e u_e} + \frac{du_e}{d \frac{x}{r_n}}\right) \tag{3}$$

where δ^*/r_n and θ/r_n are defined by

$$\frac{\delta^*}{r_n}\left(1.0 + \frac{\cos\theta_c}{2\frac{r_b}{r_n}}\frac{\delta^*}{r_n}\right) = \frac{\delta}{r_n}\int_0^{1.0}\left(1.0 - \frac{\rho u}{\rho_e u_e}\right)\left(1.0 + \frac{\frac{\delta}{r_n}\frac{y/r_n}{\delta/r_n}\cos\theta_c}{r_b/r_n}\right)d\frac{y/r_n}{\delta/r_n} \tag{4}$$

$$\frac{\theta}{r_n}\left(1.0 + \frac{\cos\theta_c}{2\frac{r_b}{r_n}}\frac{\theta}{r_n}\right) = \frac{\delta}{r_n}\int_0^{1.0}\frac{\rho u}{\rho_e u_e}\left(1.0 - \frac{u}{u_e}\right)\left(1.0 + \frac{\frac{\delta}{r_n}\frac{y/r_n}{\delta/r_n}\cos\theta_c}{r_b/r_n}\right)d\frac{y/r_n}{\delta/r_n} \tag{5}$$

Equation (3) is similar to the well-known momentum integral equation (eq. (42), Ch. 9 of ref. 10), with the exception of the additional term

$$\frac{\delta/r_n}{u_e}\left[\frac{dp_e}{d\frac{x}{r_n}}\frac{g_c}{\rho_e u_e} + \frac{du_e}{d\frac{x}{r_n}}\right] \tag{6}$$

For configurations with slight nose bluntness, a variable-entropy condition exists along the edge of the boundary layer. Therefore, the Bernoulli equation is not applicable and the previous term (eq. (6)) is added.

Velocity Profile

The velocity profiles used in the integral parameters (eqs. (4) and (5)) were calculated from the N-power law relations:

$$\frac{u}{u_e} = \left(\frac{y/r_n}{\delta/r_n}\right)^{1/N} \tag{7}$$

The value of N was calculated from a correlation of N which is a function of $R_{e,\theta}$, M_e, T_w/T_e, and $\frac{x_{vo}}{r_n}\Big/\frac{\theta}{r_n}$ shown in figure 1. The limited amount of data for N values used in the correlation were taken from turbulent velocity profiles on flat plates, cones, hollow cylinders, and shock tube walls taken from references 11 to 24 and correlate as

$$\left.\begin{aligned} N &= 6.0 \log z - 7.0 \\ \text{where} \\ z &= \frac{R_{e,\theta}^{1/3}\left(\frac{T_w}{T_e}\right)^{1/2}\left(\frac{x_{vo}/r_n}{\theta/r_n}\right)^{1/3}}{M_e^{1/4}} \end{aligned}\right\} \tag{8}$$

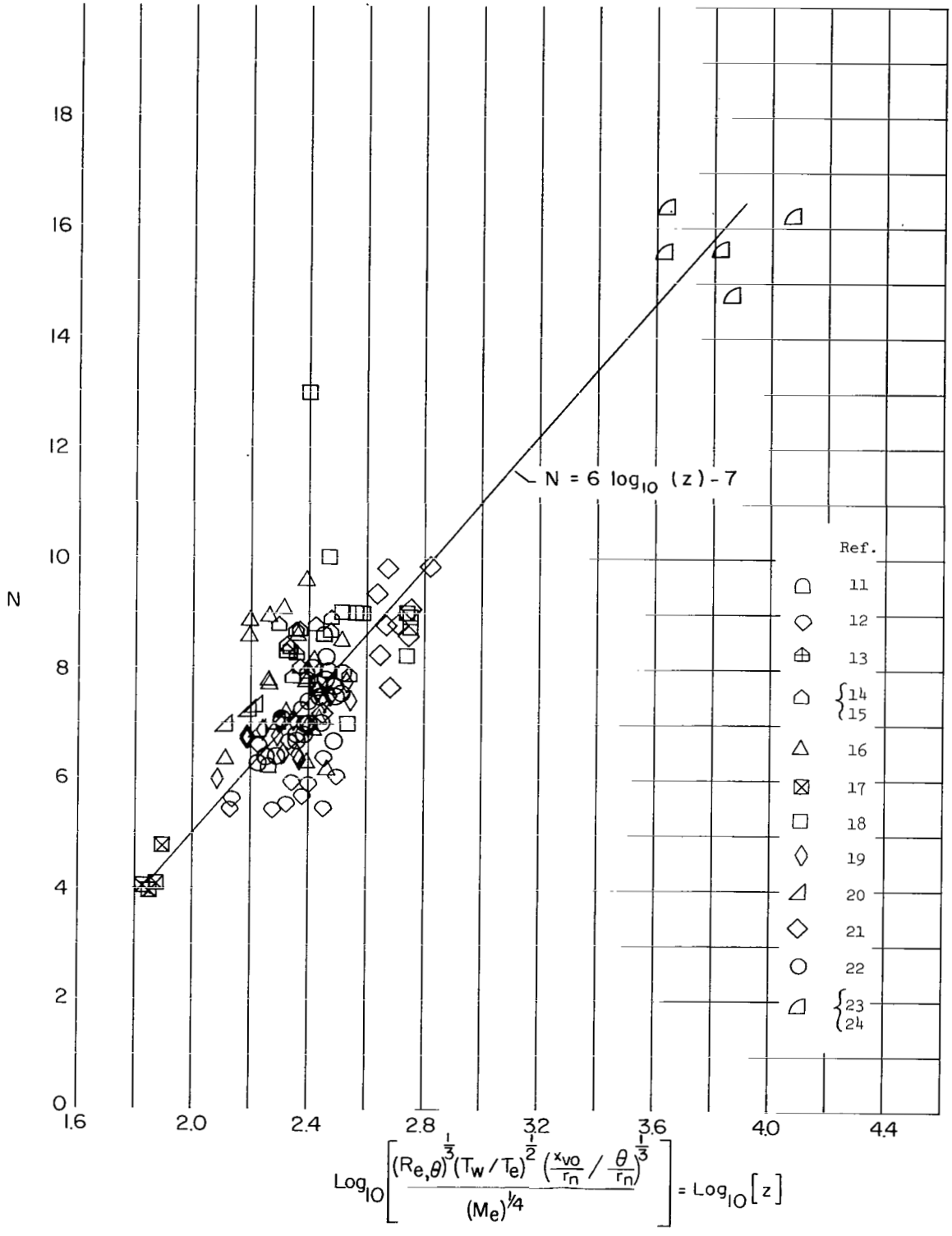

Figure 1.- Variation of the N power-law velocity-profile-exponent correlating parameter z for flat plates, cones, and hollow cylinders.

A small change in the value of N (that is, approximately ±10 percent) does not have a large effect on the calculated values of the integral parameters, δ^*/r_n and θ/r_n, provided the value of N is greater than approximately 7. In general, the overall result of the boundary-layer calculation (particularly heat transfer) is insensitive to small changes in the value of N provided the velocity profile is fully turbulent (N > 7).

The $\frac{x_{vo}}{r_n}\Big/\frac{\theta}{r_n}$ parameter used in the z correlating parameter (eq. (8)) is similar to the x/θ parameter used in the "N-power-law" correlating parameter of reference 25. The x_{vo}/r_n used in equation (8) is the dimensionless distance from the virtual origin of turbulent flow, whereas the x used in reference 25 is the distance along the nozzle center line from the throat to the measuring station. The expression used to find the virtual origin distance on a cone is

$$\frac{x_{vo}}{r_n} = \frac{\theta/r_n}{1.045\,\frac{\overline{C}_F}{2}} \tag{9}$$

where $\overline{C}_F/2$ is the Spalding-Chi (ref. 7) average value of skin friction and θ/r_n is the local value of momentum thickness. The flat plate $\overline{C}_F/2$ from reference 7, used in equation (9), is correlated for use on a cone by multiplying the $\overline{C}_F/2$ by 1.045. (See appendix.) The x_{vo}/r_n in equation (8) is always calculated from the Spalding-Chi (ref. 7) $\overline{C}_F/2$ regardless of what skin-friction law is used in equation (3), in order to be consistent with the values of x_{vo}/r_n that were used to establish the correlation in figure 1. The exponents of the parameters in z (eq. (8)) were evaluated on a trial-and-error basis for over 300 combinations until the best combination of correlating parameters was found. A more detailed survey of the "N power-law" velocity profiles is given in reference 26.

Density Profiles

Boundary-layer density profiles were calculated for equilibrium air by use of the same real-gas thermodynamic tables that were used in the inviscid calculation. (See ref. 27.) The density at a point in the boundary layer was found by entering the equilibrium air thermodynamic tables with the local static pressure and the calculated value of static enthalpy. The calculation of a density profile through the boundary layer is based on the assumption that the total enthalpy through the boundary layer varies as a function of u/u_e according to a modified form of the Crocco expression given by

$$\frac{H - h_w}{H_e - h_w} = A_R + B_R\left(\frac{u}{u_e}\right)^{\alpha_R} \tag{10}$$

The total enthalpy at any point in the boundary layer is given by

$$H = h + \frac{u^2}{2} \tag{11}$$

When equations (10) and (11) are combined, the resulting expression for static enthalpy is

$$h = h_w + (H_e - h_w)\left[A_R + B_R\left(\frac{u}{u_e}\right)^{\alpha_R}\right] - \frac{u_e^2}{2}\left(\frac{u}{u_e}\right)^2 \tag{12}$$

where the coefficients A_R and B_R and the exponent α_R vary with three regions of calculation through the boundary layer (denoted by subscripts I, II, and III) which are as follows:

Region I (wall) $(0 \leq u/u_e < 0.01)$.- The coefficients for the wall region as used in equation (12) are

$$\left.\begin{aligned} A_I &= 0 \\ B_I &= \frac{H_{aw} - h_w}{H_e - h_w} \frac{(N_{Pr})_w}{(N'_{Pr})^{2/3}} \\ \alpha_I &= 1.0 \end{aligned}\right\} \tag{13}$$

where the coefficient B_I is derived from

$$\left(\frac{d\,\frac{H - h_w}{H_e - h_w}}{d\,\frac{u}{u_e}}\right)_w \tag{14}$$

combined with the energy equation, the Fourier conduction law, and the Colburn form of the Reynolds analogy. (See ref. 28.) The prime indicates that the Prandtl number is evaluated at Eckert's reference enthalpy which is

$$h' = \frac{1}{2}(h_w + h_e) + 0.22(h_{aw} - h_e) \tag{15}$$

where $h_{aw} = h_e + N_r(H_e - h_e)$ and $N_r = 0.89$ were used. The local N'_{Pr} is found from table IV of reference 29 where the Prandtl number is tabulated as a function of temperature and pressures. The temperature used to determine the Prandtl number in reference 29 is found from the real-gas thermodynamic tables as a function of h' (eq. (15)) and the local pressure p_e.

Region III (outer) $(0.1 < u/u_e \leq 1.0)$.- The coefficients for the outer region (region III) as used in equation (10) are

$$\left.\begin{aligned} A_{III} &= 0 \\ B_{III} &= 1.0 \\ \alpha_{III} &= \text{Constant at a given } x \text{ station} \end{aligned}\right\} \tag{16}$$

(Note that $\alpha_{III} = 1.0$ for sharp flat plate and sharp or slightly blunt cones and $\alpha_{III} = 2.0$ for axisymmetric nozzles. (See ref. 8.))

Region II (intermediate) $(0.01 \leqq u/u_e \leqq 0.1)$.- Regions I and III are joined by an intermediate linear relationship which matches the region I (wall) equation at $u/u_e = 0.01$ and the region III (outer) at $u/u_e = 0.10$, where the coefficients used in equation (10) for the intermediate region are calculated from

$$\left.\begin{aligned} A_{II} &= B_{III}(0.1)^{\alpha_{III}} - 0.1B_{II} \\ B_{II} &= \frac{B_{III}(0.1)^{\alpha_{III}} - B_I(0.01)}{(0.09)} \\ \alpha_{II} &= 1.0 \end{aligned}\right\} \tag{17}$$

It should be noted that the boundaries of the three regions may be different from the values assumed herein. (See ref. 8.)

Mass Flow Into Boundary Layer

The fact that the Bernoulli equation cannot be used in the momentum equation because of a change in entropy along the edge of the boundary layer has been previously pointed out in the derivation of equation (3). There is a change in entropy between the two closely spaced streamlines passing through the shock and this change in entropy at the shock is transmitted to the edge of the boundary layer by the two streamlines. The change in entropy at the edge of the boundary layer is determined from the entropy distribution along the shock. When the entropy at the edge of the boundary layer and the static pressure distribution over the body are known, the remaining edge conditions and flow properties can be found from equilibrium air thermodynamic tables. The variation in boundary-layer edge conditions due to change in entropy may be calculated by balancing the mass flow in the boundary layer with that entering the stream tube through the shock given by

$$2\pi\left(\frac{r_s}{r_n}\right)^2 \rho_\infty u_\infty = \int_0^\delta \rho u \, dA \tag{18}$$

The expression for the shock radius is then given by

$$\frac{r_s}{r_n} = \sqrt{2 \frac{r_b}{r_n} \frac{\rho_e u_e}{\rho_\infty u_\infty} \frac{\delta}{r_n} \int_0^{1.0} \frac{\rho u}{\rho_e u_e} \left(1.0 + \frac{\frac{\delta}{r_n} \frac{y/r_n}{\delta/r_n} \cos \theta_c}{r_b/r_n} \right) d \frac{y/r_n}{\delta/r_n}} \tag{19}$$

The value of the entropy at the edge of the boundary layer is found with r_s/r_n (from eq. (19)) from a table of shock radius and shock entropy from the inviscid calculation.

Skin-Friction Calculation

A value of the local coefficient of skin friction is needed at each point of calculation in order to evaluate the right-hand side of equation (3). In addition to its use in the solution of the integral momentum equation, the local skin-friction coefficient may be used to obtain local heat transfer by using the Reynolds analogy to obtain a local Stanton number. In reference 30 a comparison has been made of four turbulent skin-friction theories with experimental data. The results of the comparison indicated that the skin-friction laws of Van Driest II (that is, Karman mixing length, ref. 31) and Spalding-Chi (ref. 7) gave reasonably good agreement with heat-transfer data over $0.1 < T_w/T_t \leq 1.0$ when the Reynolds analogy factor $\left(\text{that is, } \frac{N_{St,e}}{C_{f/2}}\right)$ was 1.0 for the Van Driest II theory and 1.16 for the Spalding-Chi theory. The calculation of the Van Driest II theory in reference 30 (described in detail in ref. 6) uses a Karman-Schoenherr incompressible skin-friction expression. The Karman-Schoenherr equation uses a transformed value of the local Reynolds number based on momentum thickness to obtain skin-friction coefficient for the incompressible plane. The skin-friction coefficient for the incompressible plane is transformed to the compressible plane by using an expression which is a function of M_e, and T_w/T_e, and is analogous to the Spalding-Chi F_c function. (See ref. 7.) This analogous F_c function is referred to as the "Van Driest II F_c function" and is given in reference 6 as

$$F_c = \frac{0.176 M_e^2}{\sin^{-1}\alpha + \sin^{-1}\beta} \tag{20}$$

where α and β are functions of Mach number and temperature ratio. (See ref. 6.)

It should be noted that the Van Driest II and the Spalding-Chi skin-friction theories presented in reference 6 use the same expression to obtain the incompressible skin friction and also use the same F_c function (eq. (20)) to transform the incompressible skin friction to the compressible plane. The F_c function given in reference 6 uses the linear Crocco in its derivation $\left(\text{that is, } A_R = 0,\ B_R = 1.0,\ \alpha_R = 1.0 \text{ in eq. (10)}\right)$. The skin-friction calculations made in this report by using the Spalding-Chi theory used the

F_c function as given in reference 7. The general expression given in reference 7 for F_c is

$$F_c = \left[\int_0^1 \left(\frac{\rho}{\rho_e}\right)^{1/2} d\,\frac{u}{u_e}\right]^{-2} \tag{21}$$

The F_c function given in equation (21) may be integrated by using a real-gas variation of equation (12); however, the correct values of α_R must be used. The ideal gas F_c function used in reference 7 to correlate the skin-friction data is given by

$$F_c = \left(\int_0^1 \frac{d\,\frac{u}{u_e}}{\left\{\frac{T_w}{T_e} + \left[1 + \frac{N_r}{2}(\gamma - 1)M_e^2 - \frac{T_w}{T_e}\right]\frac{u}{u_e} - \frac{N_r}{2}(\gamma - 1)M_e^2\left(\frac{u}{u_e}\right)^2\right\}^{1/2}}\right)^{-2} \tag{22}$$

where N_r, as used in reference 7, is equal to 0.89. Equation (22) was derived from equation (21) with the assumption of a linear Crocco relationship (that is, $\alpha_R = 1.0$). The local skin-friction coefficient obtained from the turbulent-flat-plate theories from either reference 7 or reference 6 must be corrected for application to a cone by the Mangler transformation factor F_{MT}. (See appendix.) The local skin friction on a cone downstream of the end of transition is found from

$$\left(\frac{C_f}{2}\right)_{Cone} = F_{MT}\left(\frac{C_f}{2}\right)_{Flat\ plate} \tag{23}$$

where for fully turbulent flow

$$F_{MT} = 1.176 \tag{24}$$

The determination of the local value of skin friction from the Spalding-Chi (ref. 7) and Van Driest II (ref. 6) theories is calculated by use of a Reynolds number based on momentum thickness rather than on a Reynolds number based on a surface distance. The use of $R_{e,\theta}$ to find $C_f/2$ (1) eliminates the necessity of establishing a virtual origin of the turbulent flow and (2) makes use of the momentum thickness which is calculated directly from the momentum integral equation (eq. (3)). It is recognized that a pressure and entropy gradient can affect C_f; however, this effect has been neglected in the present work.

Transition Region

The value of $C_f/2$ in the transition region is assumed to vary as

$$\frac{C_f}{2} = \frac{C_f}{2}\bigg|_{tr} + \frac{Y}{2 \tanh \psi}\left[\left(\frac{C_f}{2}\right)_{turb} - \left(\frac{C_f}{2}\right)_{tr}\right] \tag{25}$$

where

$$Y = \tanh \psi + \tanh X$$

$$X = \psi - 2\psi\left[\frac{\left(\frac{x}{r_n}\right)_{turb} - \frac{x}{r_n}}{\left(\frac{x}{r_n}\right)_{turb} - \left(\frac{x}{r_n}\right)_{tr}}\right]$$

and ψ = Constant. The value of ψ controls the degree of nonlinearity of $C_f/2$ with respect to x/r_n in the transition region and for all calculations the value ψ was equal to 2.0. The variation of $C_f/2$ in the transition region as calculated from equation (25) resulted in S-shaped curves which are characteristic of variations in body $C_f/2$ and heat-transfer data in transition regions. The initial value of skin friction at the start of transition $\left(C_f/2\right)_{tr}$ may be taken from a solution for laminar flow or from a value based on experimental data. The value of skin friction at the end of transition $\left(C_f/2\right)_{turb}$ is calculated from the turbulent value found from equation (23).

The value of N in the transition region is assumed to vary as

$$N = N_{tr} + \frac{Y}{2 \tanh \psi}\left(N_{turb} - N_{tr}\right) \tag{26}$$

where Y is the expression used in equation (25) and $\psi = 2.0$. The value of N_{tr} is taken from the theoretical laminar calculation. The value of N at the end of the transition N_{turb} is calculated from equation (8).

The value of α_{III} used in equation (12) varies linearly from an initial value at the start of transition to $\alpha_{III} = 1.0$ at the end of the transition region.

Heat Transfer

The local Stanton number is calculated from a modified Reynolds analogy in the form

$$N_{St,e} = \frac{C_f}{2} R_{AF} \tag{27}$$

where R_{AF} is the Reynolds analogy factor. The value of the R_{AF} depends on which local turbulent skin-friction theory is used. If the Van Driest II (ref. 6) is used for heat

transfer, the Reynolds analogy factor is a function of h_w/H_e as listed in table I and for the Spalding-Chi skin-friction theory (ref. 7), $R_{AF} = \frac{1}{(N'_{Pr})^{2/3}}$.

TABLE I.- VARIATION OF REYNOLDS ANALOGY FACTOR WITH h_w/H_e

h_w/H_e	R_{AF}
$\frac{h_w}{H_e} < 0.2$	1.0
$0.2 \leqq \frac{h_w}{H_e} \leqq 0.65$	$0.8311 + 0.9675 \frac{h_w}{H_e} - 0.6142\left(\frac{h_w}{H_e}\right)^2$
$\frac{h_w}{H_e} > 0.65$	1.2

The variation of the Reynolds analogy in table I is based on the results of references 32, 33, and 30 which indicated a decrease in R_{AF} with a decrease in h_w/H_e. The results in reference 32 show considerable scatter in the data; however, there is a definite decrease in the value of the R_{AF} with a decrease in h_w/H_e based on a least-squares curve fit of the data. The value of R_{AF} from the experimental data of reference 33 showed a marked decrease for a h_w/H_e ratio below 0.3. In reference 30 $R_{AF} \approx 1.0$ $(N_r = 0.9)$ was found for a simultaneous measurement of skin friction and heat transfer. Additional heat-transfer data in reference 30 indicate an increase in R_{AF} as T_w/T_t increases similar to those of references 32 and 33. When the Spalding-Chi (ref. 7) theory was used in equation (27), $R_{AF} = (N'_{Pr})^{-2/3}$ (that is, Colburn's modified form of Reynolds analogy) was found to give the best prediction of heat transfer. The value of N'_{Pr} is taken from tables of Prandtl number given in reference 29 evaluated at h' (see eq. (15)) and the local static pressure.

The local heat-transfer coefficient $\bar{h}$ is calculated from

$$\bar{h} = N_{St,e} u_e \rho_e \tag{28}$$

The heating rate q is calculated from

$$q = \bar{h}(h_{aw} - h_w) \tag{29}$$

where $h_{aw} = h_e + N_r(H_e - h_e)$ where $N_r = 0.89$.

A constant value of $N_r = 0.89$ through the transition region is not correct; however, for cold wall calculations (that is, h_w negligibly small compared with H_e), the maximum error at the start of transition is approximately 4 percent. When the wall

temperature becomes significant compared with the adiabatic wall temperature, the variation of N_r should be included in equation (29). A summary of several of the parameters used in calculation of the transitional and turbulent boundary is given in table II.

TABLE II.- SUMMARY OF PARAMETERS USED IN TWO REGIONS OF CALCULATION

Parameter	Initial value at start of transition	Transitional boundary layer	Turbulent boundary layer
N	Laminar profile	Equation (26)	Equation (8)
α_{III}	Laminar profile	Linear variation from laminar value at start to 1.0 at the end of transition region	$\alpha_{III} = 1.0$
$C_f/2$	Laminar value (initial value is arbitrary; any value may be used)	Equation (25)	Equation (23) (Van Driest II (ref. 6) or Spalding-Chi (ref. 7))
Mangler transformation factor (F_{MT})	Not applicable	Not used (see eq. (25))	(Used in eq. (23)) Van Driest II – 1.176 (eq. (33)) Spalding-Chi (eq. (34))
Reynolds analogy factor (R_{AF})	The basis for the R_{AF} is the same for the transitional and turbulent region, that is, Van Driest: Table I Spalding-Chi: $(N'_{Pr})^{-2/3}$		

METHOD OF CALCULATION

The general method of calculation using the Langley Research Center computer program D-3340 is an iterative procedure which requires a calculation from the beginning of transition to the end of the body to be repeated until the velocity at the edge of the boundary layer changes less than 1 percent from one iteration to the next. When the velocity change is less than 1 percent, the calculation is terminated. The calculation procedure first requires an inviscid solution (see refs. 27 and 34) followed by a viscous solution which uses the wall conditions at the $y = 0$ boundary conditions and the results from the inviscid solution to establish the initial boundary conditions at the outer edge of the boundary layer. The conditions at the outer edge of the boundary layer change as the entropy at the edge of the boundary layer decreases from the stagnation value as a result of the mass flow into the boundary layer. If sufficient mass enters the boundary layer, the entropy at the edge will approach the sharp-cone value. The radius of the stream tube at the shock is determined from mass flow considerations. (See eq. (19).) The entropy at the edge of the boundary layer is determined from a table of shock radius against entropy as calculated from the inviscid solution. The viscous solution is then

inserted between the body and the inviscid solution, the assumption being that the displacement thickness correction does not change the effective body shape. Since there is no computed change in the effective body shape, the original pressure distribution and shock shape from the inviscid calculation do not change as a result of the viscous calculation. The flow properties at the edge of the boundary layer are determined from real-gas thermodynamic tables by using the pressure distribution and entropy at the boundary-layer edge to enter the table.

Thermodynamic Properties for a Real Gas

The flow properties in the viscous and inviscid flow fields, such as p_e, ρ_e, T_e, S_e, h_e, a_e, etc., are calculated from the equilibrium air thermodynamic computer subroutine described by Lomax and Inouye for an inviscid solution in reference 27. During the calculation, thermodynamic data at a point are found by entering the real-gas subroutine with pressure and entropy. For calculations of density profiles through the boundary layer, the real-gas calculation is modified to allow the thermodynamic data to be found for a given enthalpy (or temperature) and pressure. The procedure in this case is to enter the real-gas subroutine with various estimated values of entropy and the local pressure until the value of entropy is found that yields the desired value of enthalpy (or temperature).

Calculating Procedure

Prior to the boundary-layer calculation, the inviscid flow field is determined by the Lomax and Inouye blunt-body and method-of-characteristics programs. (See refs. 27 and 34.) The inviscid solution gives the first-order stagnation entropy flow property distribution along the body which is used as the initial conditions at the edge of the boundary layer. In addition, the shock shape r_s/r_n and entropy distribution along the shock are found from the inviscid solution. The results of the inviscid solution are first used to make a laminar boundary-layer calculation, with variable entropy, over the entire length of the body. (See ref. 35.) The turbulent boundary-layer calculations then follow. As previously noted, the pressure distribution over the body does not change as a result of the viscous calculation; however, all other conditions at the edge of the boundary layer change because of the change in local entropy. The turbulent-boundary-layer calculation is initiated at the point where transition has been determined to start. The initial edge conditions used in the turbulent-boundary-layer calculation come from the laminar solution. The initial use of the edge conditions from the variable-entropy solution for laminar flow enables the turbulent calculation to be completed in less time than the initial use of the stagnation entropy edge conditions directly from the inviscid solution. Specifically, the output from the solution with variable entropy for laminar flow gives tables of r_s/r_n,

and dimensionless shear as a function of x/r_n which are used for input to the turbulent-boundary-layer calculation. An initial entropy distribution at the edge of the boundary layer used in the first iteration for turbulent flow is determined from the table of r_s/r_n against x/r_n from the solution for laminar flow and the inviscid entropy distribution along the shock. At the point where the laminar-boundary-layer calculation stops and the transitional-boundary-layer calculation starts, the dimensionless shear table is used to find the initial value of $C_f/2$ and the r_s/r_n table is used to find an initial value of r_s/r_n. The value of r_s/r_n at the start of transition specifies a value of entropy; with this value of entropy and the local static pressure, the flow conditions at the edge of the boundary layer are known by entering the real-gas subroutine with entropy and pressure. The initial values of the velocity and density profile are based on the laminar profiles from which values of N and α_{III} are determined, just upstream of the start of transition. Nominally, the initial value of N is 1.5 and α_{III} is 1.0. Downstream of the end of transition, α_{III} is held constant (usually a value of 1.0). The value of the boundary-layer thickness at the start of transition is calculated from equation (19) by use of the initial value of r_s/r_n, N, and α_{III}. The initial values of θ/r_n and δ^*/r_n are found from equations (5) and (4), respectively. Downstream of the initial point of calculation, the value of θ/r_n is calculated from the integration of equation (3), and δ/r_n and δ^*/r_n are calculated from equations (5) and (4), respectively.

Transition Region

The region from the end of the laminar-flow solution (beginning of turbulent solution) to the point where the solution is considered to be fully turbulent is defined as the transition region. A guide for the selection of the length of the transition region, based on experimental data, is that the transition region ends when the local Reynolds number is approximately twice its value at the beginning of the transition region. (See ref. 36.) However, the guideline of a factor of two in $R_{e,x}$ for the end of transition is not always applicable when the edge conditions are changing very rapidly in the transition region because of the variable-entropy effects. These effects cause an increase in Reynolds numbers in the transition region which may be considerably different from a factor of 2.0. Therefore, the location of the end of transition was put into the calculation as a specific value. The calculation procedure in the transition region is the same as the fully turbulent solution with three exceptions (see table II): (1) the value of N in the transition region is calculated from equation (26); (2) the value of $C_f/2$ in the transition region is determined from equation (25); and (3) the value of α_{III} varies from an initial value at the start of transition to value of 1.0 at the end of transition. After each calculation (iteration), from the start of transition to the end of the body, the relationship in the transition region for N and $C_f/2$ as a function of x/r_n (eqs. (25) and (26)) is recalculated for use in the next iteration.

Computer Calculation Time

The time required for a given variable-entropy calculation for turbulent flow depends on (1) the number of iterative calculations from the start of transition to the end of the body; (2) the number of points on the body per iteration; (3) the number of points in the integration from the wall to the edge of the boundary layer; and (4) the error criterion for various iterative solutions used in the calculation. It usually took four iterations to find a reasonable engineering solution which had a change in velocity of less than 1 percent $\left(\frac{\Delta u_e}{u_e} < 0.01\right)$ from one iteration to the next. For the flight calculation, the Runge-Kutta integration was limited to maximum step size of $\frac{x}{r_n} = 16.0$; however, if calculation time on the computer is extremely critical, the step size could possibly be increased with little effect on the final solution. The number of points required in the Gaussian quadrature for the calculation of δ/r_n and δ^*/r_n from equations (5) and (4), respectively, was determined from a comparison of the values of δ/r_n and δ^*/r_n calculated for various numbers of points used in the quadrature. It was determined that a minimum number of 20 points could be used in the integration through the boundary layer. The momentum integral equation (eq. (3)) is solved by a variable-step-size fifth-order Runge-Kutta numerical scheme which uses a maximum relative error criterion of 0.001 for the value of θ for one step of integration. The maximum percent error allowed in the iterative solution for the Spalding-Chi (ref. 7) $C_f/2$ was 0.4. When an iterative procedure had to be used in the determination of thermodynamic properties from the real-gas subroutine (see ref. 27), the maximum allowable relative error was 0.001. For real-gas turbulent-boundary-layer calculations made at altitudes from 18.29 km to 25.91 km (60 000 ft to 85 000 ft) at $M \approx 20$, the time per point of calculation was approximately 2.6 seconds on the Control Data 6600 computer system based on a single iteration from the start of transition to the end of the body and using the relative error criteria.

RESULTS AND DISCUSSION

Comparison of Ground Test Data and Theoretical Predictions of Heat Transfer

In order to evaluate the integral theory in terms of its ability to predict heat transfer, a comparison was made between theoretical and experimental results for three sets of heat-transfer data.

Flat-plate data.- In figure 2 six integral calculations of Stanton number were made in order to evaluate the effect of α_R and F_c (see eq. (12)) on the integral method when the skin-friction laws of Spalding-Chi (ref. 7) and Van Driest II (ref. 6) are used. Four calculations using the Spalding-Chi skin-friction theory were made for two F_c functions

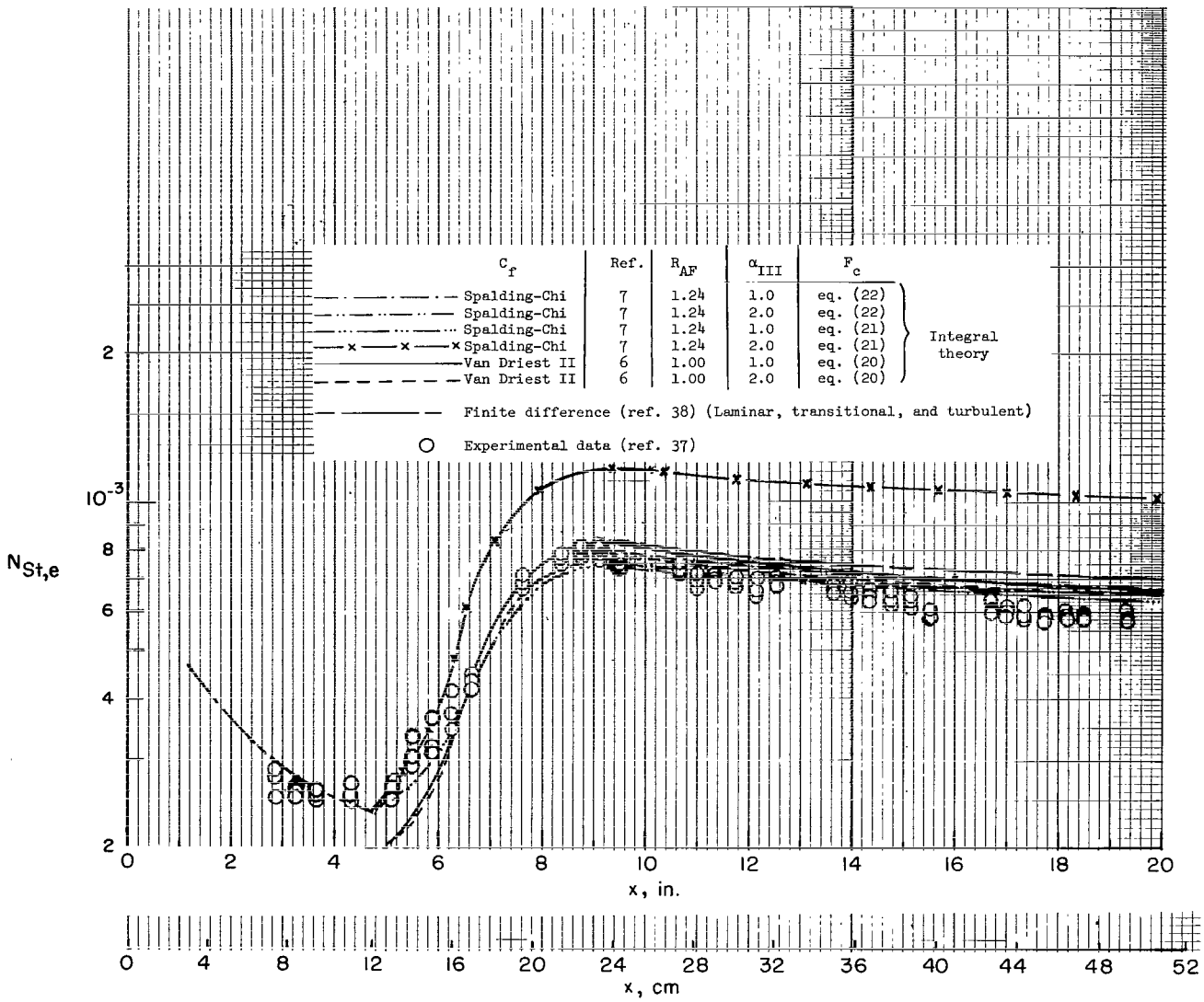

Figure 2.- A comparison of heat-transfer data on a flat plate with integral and finite-difference methods of prediction at Mach 6.0 and $\frac{T_w}{T_t} = 0.2$.

(eqs. (21) and (22)) with α_R equal to 1.0 and 2.0 for both methods of obtaining F_c. The other two calculations were made with the Van Driest II skin-friction theory, by using equation (20) for the F_c function, with values of α_R of 1.0 and 2.0. The six integral calculations are compared in figure 2 with the heat-transfer data at $\frac{T_w}{T_t} = 0.2$ of reference 37. Five of the theoretical predictions, which use a linear Crocco relationship to derive the F_c equation, agree well with the data at peak heating but tend to overpredict by approximately 10 percent at the 50.8-cm (20-in.) station. The sixth Stanton number calculation from the Spalding-Chi theory, which uses $\alpha_R = 2.0$ to integrate the basic expression for F_c (eq. (21)), predicts a Stanton number which is approximately

70 percent above the data. In general, the results of the integral calculations show that when the F_c function is derived for a linear Crocco relationship (that is, $\alpha_R = 1.0$, eqs. (20) and (22)), the heat-transfer prediction is close to the data even though the integral parameters are calculated for $\alpha_R = 2.0$. Therefore, if equation (21) is to be integrated for either an ideal gas or a real-gas variation of density through the boundary layer, evidently an $\alpha_{III} = 1.0$ must be used. In addition, the predictions calculated from the finite-difference theory of reference 38 for both the laminar and turbulent flow are in general agreement with the five integral predictions.

Blunt-cone data.- Two sets of heat-transfer data are used as a basis of comparison for heat-transfer predictions with variable entropy and are shown in figures 3 and 4. The

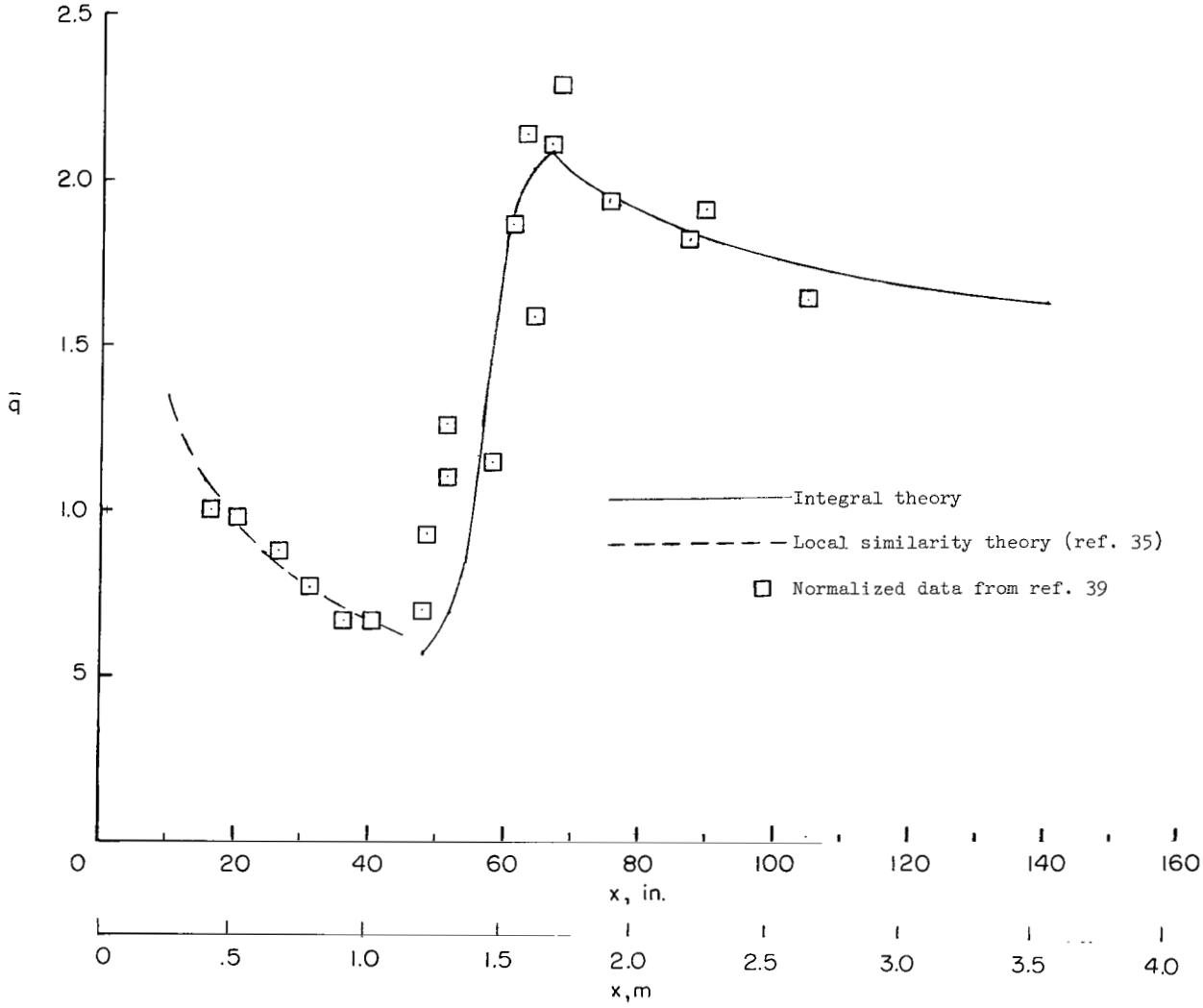

Figure 3.- A comparison of normalized heating-rate predictions from the final iterations for laminar and turbulent boundary layers to experimental wind-tunnel data at $M_\infty = 11.5$ on a 5° half-angle cone at $R = 8.5 \times 10^6/m$ $(2.6 \times 10^6/ft)$. $r_n = 2.54$ mm (0.10 in.).

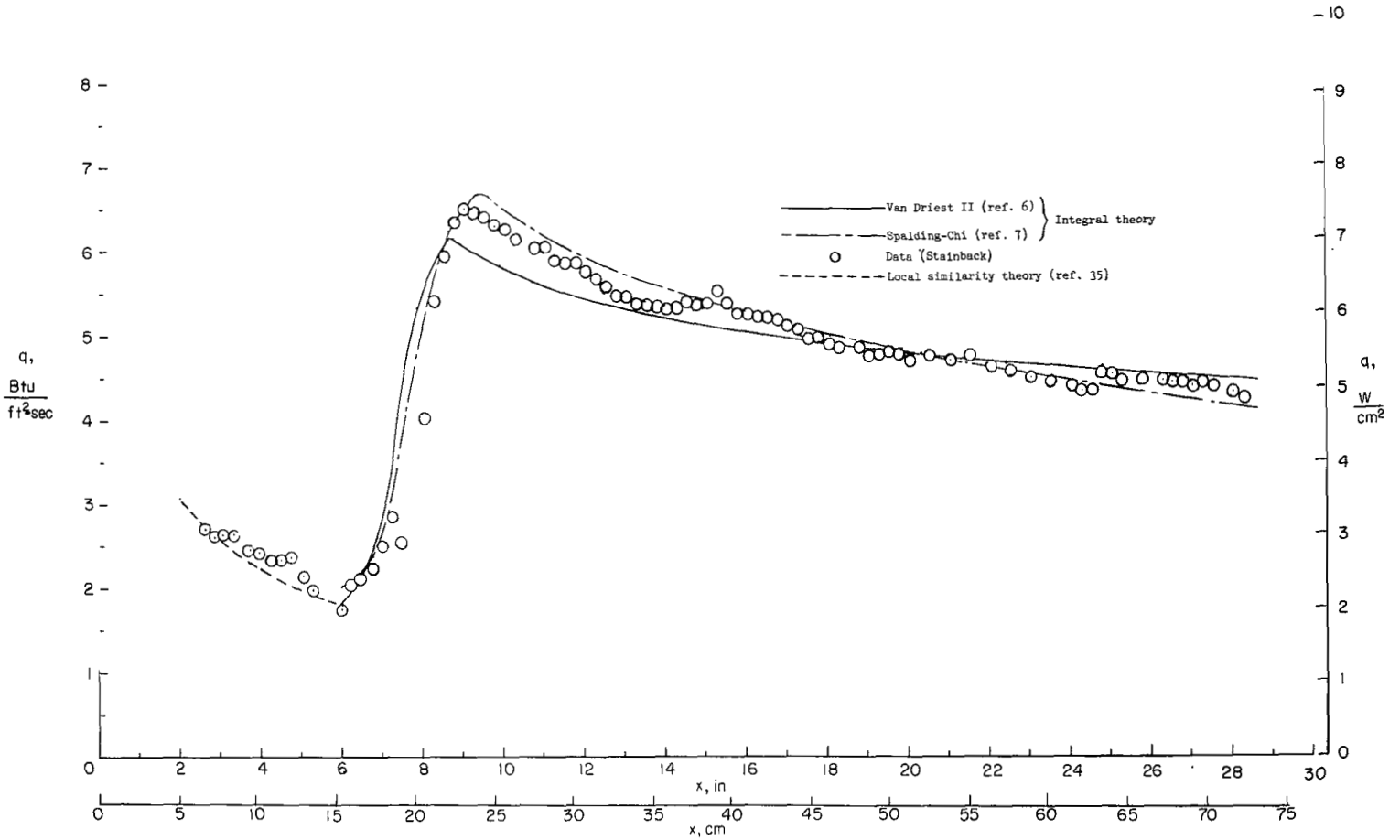

Figure 4.- A comparison of heating-rate predictions from the final iterations for laminar and turbulent boundary layers to experimental wind-tunnel data at $M_\infty = 8.0$ on a 5° half-angle cone at $R = 43.1 \times 10^6/m$ ($13.14 \times 10^6/ft$). $r_n = 0.508$ mm (0.020 in.).

data from reference 39, shown in figure 3, were measured in a "shock tunnel" at a free-stream Mach number of 11.5 on a 3.66-meter-long (12-ft), 5° half-angle cone, with a 0.254-cm (0.10-in.) nose radius. The data (ref. 39) in figure 3 were normalized in order that the laminar data match the theoretical prediction for laminar flow (ref. 35) at x = 50.8 cm (20 in.). When the data from reference 39 are normalized, the theoretical prediction in figure 3 for both laminar flow (ref. 35) and the integral theory for turbulent flow, presented in this paper, agree reasonably well.

A comparison between data obtained by P. Calvin Stainback of Langley Research Center and theoretical predictions from two integral methods, using Spalding-Chi (ref. 7) and Van Driest II (ref. 6) are shown in figure 4. The data were taken on a 73.66-cm-long (29-in.), 5° half-angle cone with 0.508-mm (0.020-in.) nose radius. The tests were at a free-stream Mach number of 8.0 and a unit Reynolds number of 5.44×10^7 per meter (1.658×10^7 per ft). The heating-rate data in the region of turbulent flow in figure 4 is considered to be reliable because of the accurate measurements of total temperature, wall temperature, and skin thickness, and also because of the proven data reduction method for obtaining the heating rate from the rate of change of the wall temperature. (See ref. 40.) The cone used in the tests had a circumferential rearward-facing step 0.254-mm (0.010-in.) high at a station 3.81 cm (1.5 in.) from the nose. The purpose of the step was to simulate a flight configuration. The combination of the rearward-facing step and the uncertainty in the skin thickness in the small nose piece are believed to be the reasons that the laminar theory (ref. 35) slightly underpredicts the data upstream of the 15.24-cm (6.0-in.) station. In figure 4 the calculation of heat transfer in the region of peak heating for fully turbulent flow which uses the Spalding-Chi skin-friction theory (ref. 7) slightly overpredicts the data; whereas in the same region the Van Driest II (ref. 6) theory slightly underpredicted the data. The difference in the prediction in peak heating is a result of the two theories using different variations of F_{MT} in the turbulent flow region. The Van Driest II skin-friction theory used $F_{MT} = 1.176$ over the entire turbulent flow region whereas the Spalding-Chi theory uses equation (34) (see appendix) to obtain the variation of F_{MT}. At the end of the cone, both skin-friction laws use $F_{MT} = 1.176$ and both theories are in reasonably close agreement. The R_{AF} used with the Van Driest II skin-friction theory is given in table I, and the Spalding-Chi skin-friction theory uses $R_{AF} = \left(N'_{Pr}\right)^{-2/3}$.

Variable Entropy Turbulent Boundary Layer – Sample Flight Calculations

The results of a real-gas variable-entropy turbulent-boundary-layer calculation made for sample flight conditions are shown in figures 5 to 17. The sample calculations herein were made for a blunt 5° half-angle cone with a 1.016-cm (0.4-in.) nose radius at an altitude of 18.29 km (60 000 ft) at a velocity of 5.80 km/sec (19 019 ft/sec). The

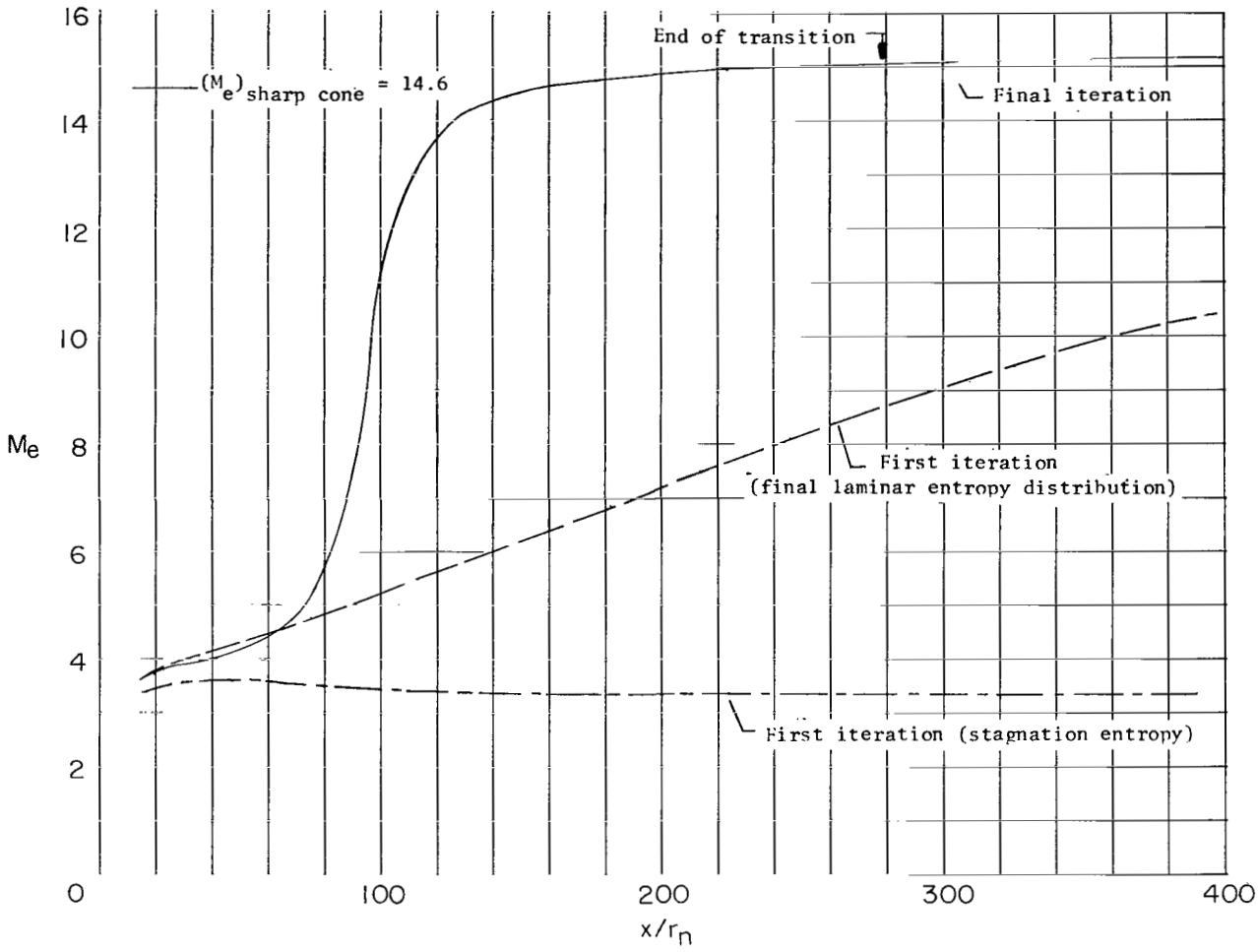

Figure 5.- The effect of three entropy distributions at the edge of the boundary layer on the local Mach number for three turbulent-boundary-layer calculations at 18.29 km (60 000 ft) and u_∞ = 5.80 km/sec (19 019 ft/sec). r_n = 1.016 cm (0.4 in.).

sample calculations for the turbulent boundary layer on a 3.96-meter-long (13-ft) cone were made with the assumption that the boundary layer was nearly turbulent over the entire body. However, in order to simulate the actual method of calculation, a short distance of laminar boundary layer was assumed to precede the start of the turbulent calculation. For the illustrative sample calculation, the start and end of transition were assumed to be $\frac{x}{r_n} = 15.0$ and $\frac{x}{r_n} = \frac{\partial 79}{223}$, respectively. The assumption of the extremely long transition region was based on the combined effects of (1) bluntness and (2) the variable entropy. Both of these effects are accentuated by the far upstream location of the start of transition. The turbulent-boundary-layer calculations in figures 5 to 15 show the results for three sets of flow properties at the edge of the boundary layer, hereafter referred to as edge conditions. The three edge conditions used in the calculation resulted

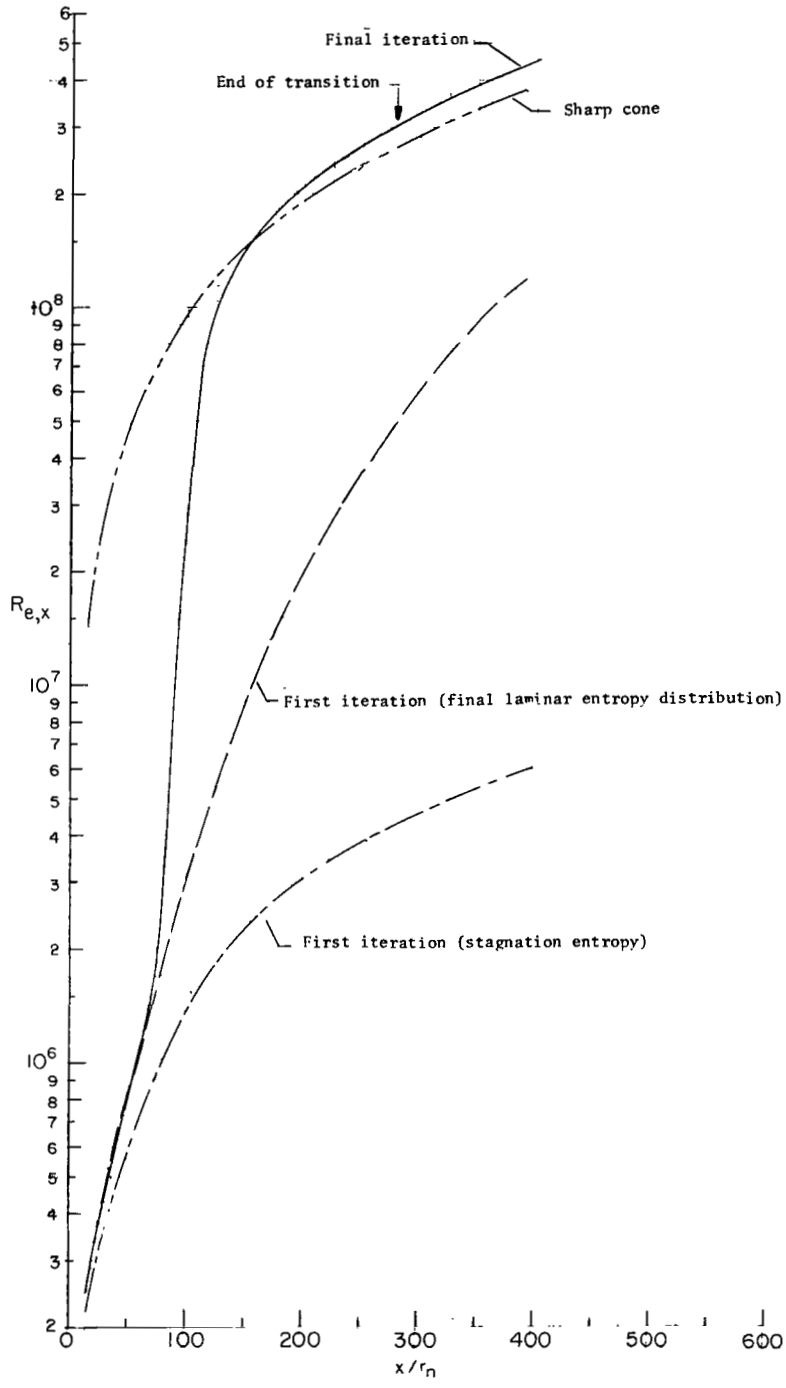

Figure 6.- The effect of three entropy distributions at the edge of the boundary layer on the local Reynolds number for three turbulent-boundary-layer calculations at 18.29 km (60 000 ft) and u_∞ = 5.80 km/sec (19 019 ft/sec). r_n = 1.016 cm (0.4 in.).

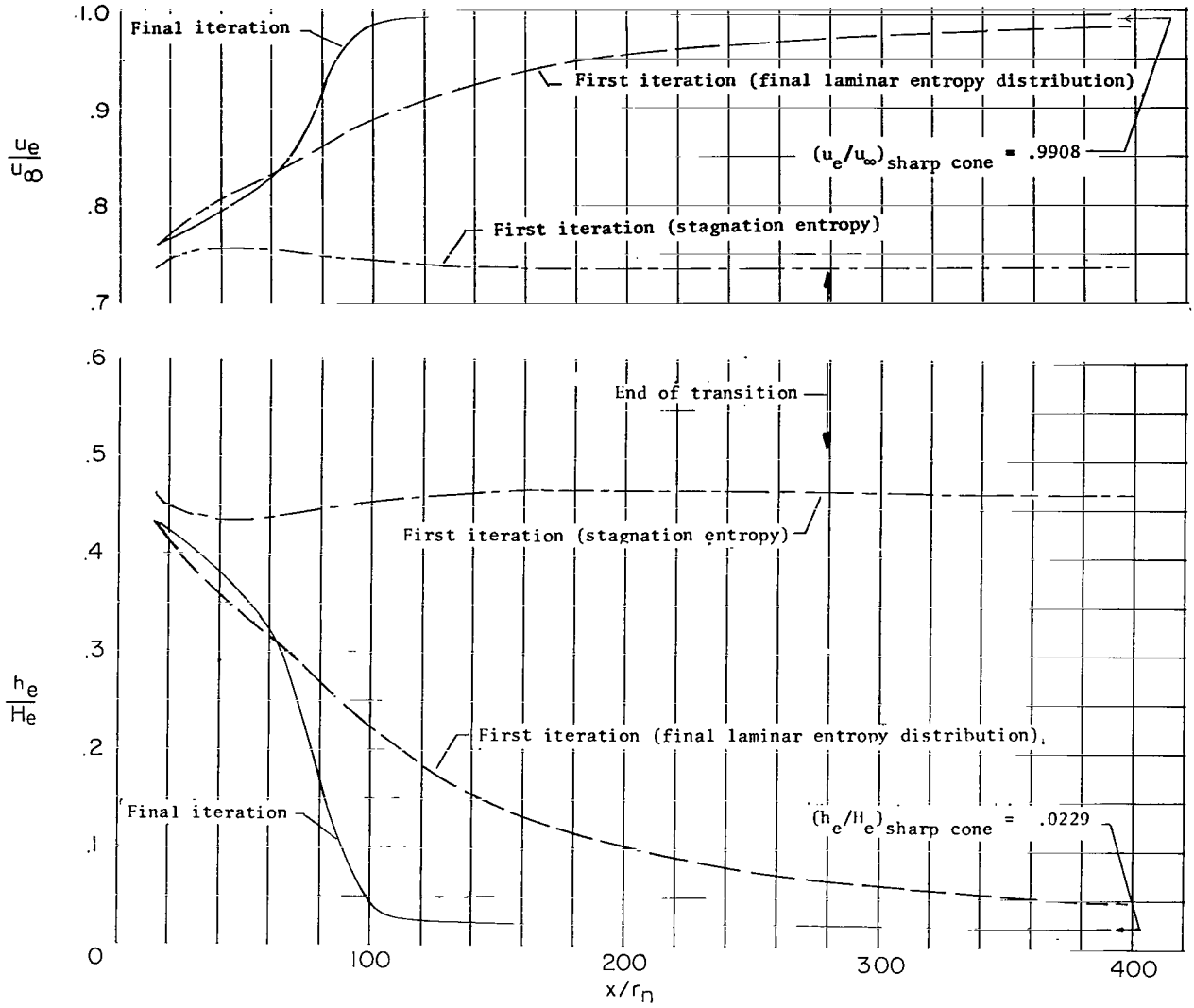

Figure 7.- The effect of three entropy distributions at the edge of the boundary layer on (1) the ratio of the local static enthalpy to the inviscid flow field total enthalpy and (2) the ratio of local velocity to free-stream velocity for three turbulent-boundary-layer calculations at 18.29 km (60 000 ft) and u_∞ = 5.80 km/sec (19 019 ft/sec). r_n = 1.016 cm (0.4 in.).

from the following three entropy distributions at the edge of the boundary layer: (1) constant stagnation entropy; (2) the entropy from the final laminar solution (see ref. 35); and (3) the entropy resulting from the final turbulent calculation. For the variable-entropy calculations for a turbulent boundary layer described in this paper, the calculation for the first iteration uses the entropy distribution resulting from the final iteration for a variable-entropy solution for laminar flow instead of using the stagnation-entropy distribution. The stagnation-entropy results are presented to illustrate the results that would be obtained if variable entropy were not considered in the calculation.

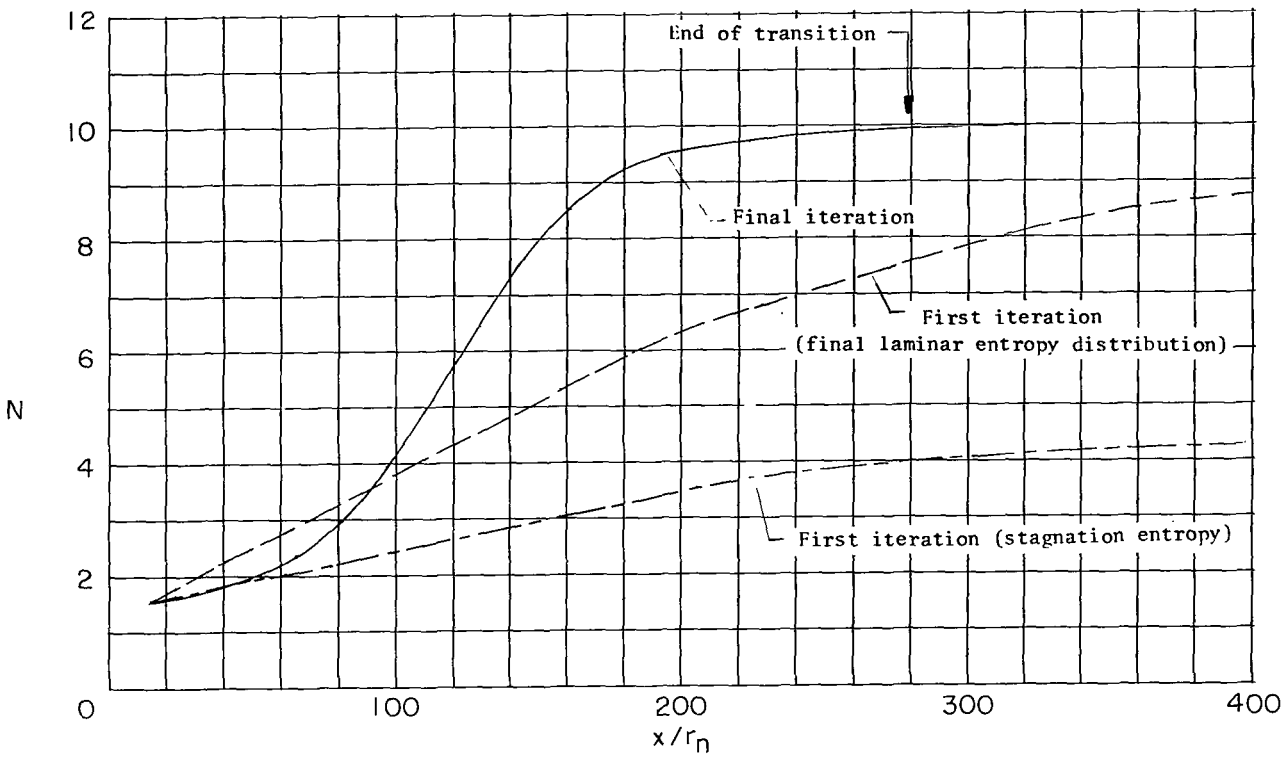

Figure 8.- The effect of three entropy distributions at the edge of the boundary layer on the value of the N power-law exponent for three turbulent-boundary-layer calculations at 18.29 km (60 000 ft) and u_∞ = 5.80 km/sec (19 019 ft/sec). r_n = 1.016 cm (0.4 in.).

Flow properties at edge of boundary layer.- The effects of the three entropy distributions on the Mach number, the Reynolds number, and the h_e/H_e ratio at the edge of the boundary layer are shown in figures 5, 6, and 7, respectively. The variation of the Mach number at the edge of the boundary layer, shown in figure 5, ranges from a value of approximately 3.6 at the upstream end of the cone to a downstream value of approximately 15.1 for the final iteration for turbulent flow. Thus, at these flight conditions a sharp-cone value of $M_e = 14.6$ is reached in the final calculation for turbulent flow at an x/r_n of approximately ~~265~~ 165, but downstream of $\frac{x}{r_n} = $ ~~265~~ 165, the Mach number overshoots the sharp-cone value of 14.6. The overshoot in the local Mach number is a result of low-entropy air (that is, less than the sharp-cone value) entering the boundary layer in a region where the surface pressure is at approximately a sharp-cone value. If the cone were long enough, the local value of Mach number would decrease gradually and become asymptotic to the sharp-cone value of 14.6.

The effect of variable entropy at the edge of the boundary layer on the local Reynolds number based on x/r_n distance is shown in figure 6. The value of $R_{e,x}$ from the final calculation for turbulent flow at the end of the cone increases by a factor of approximately 72 compared with the value found for the stagnation entropy at the same x/r_n location.

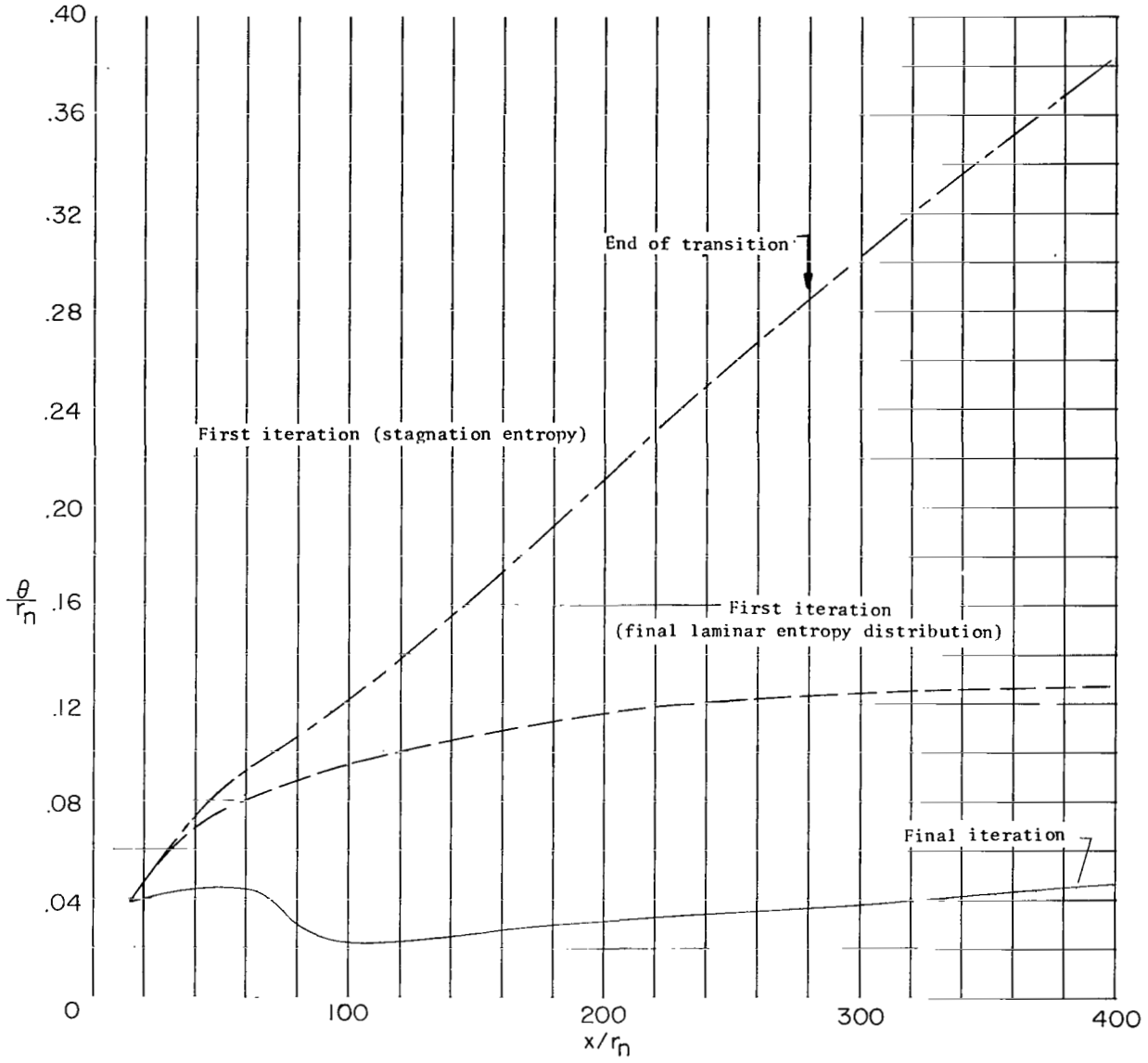

Figure 9.- The effect of three entropy distributions at the edge of the boundary layer on the momentum thickness for three turbulent-boundary-layer calculations at 18.29 km (60 000 ft) and u_∞ = 5.80 km/sec (19 019 ft/sec). r_n = 1.016 cm (0.4 in.).

The $R_{e,x}$ for the final turbulent calculation is equal to the sharp-cone value at $\frac{x}{r_n} \approx \frac{165}{\cancel{265}}$ and for $\frac{x}{r_n} > \frac{165}{\cancel{265}}$ the value of $R_{e,x}$ overshoots the sharp-cone value as was found in figure 5. Again if the cone were long enough, the value of $R_{e,x}$ from the final calculation would approach the sharp-cone value.

The effect of variable entropy on the local static enthalpy and local velocity is shown in figure 7. The h_e/H_e ratio at the end of the cone for the final turbulent calculation is approximately 20 times less than the h_e/H_e ratio calculated from the stagnation-entropy

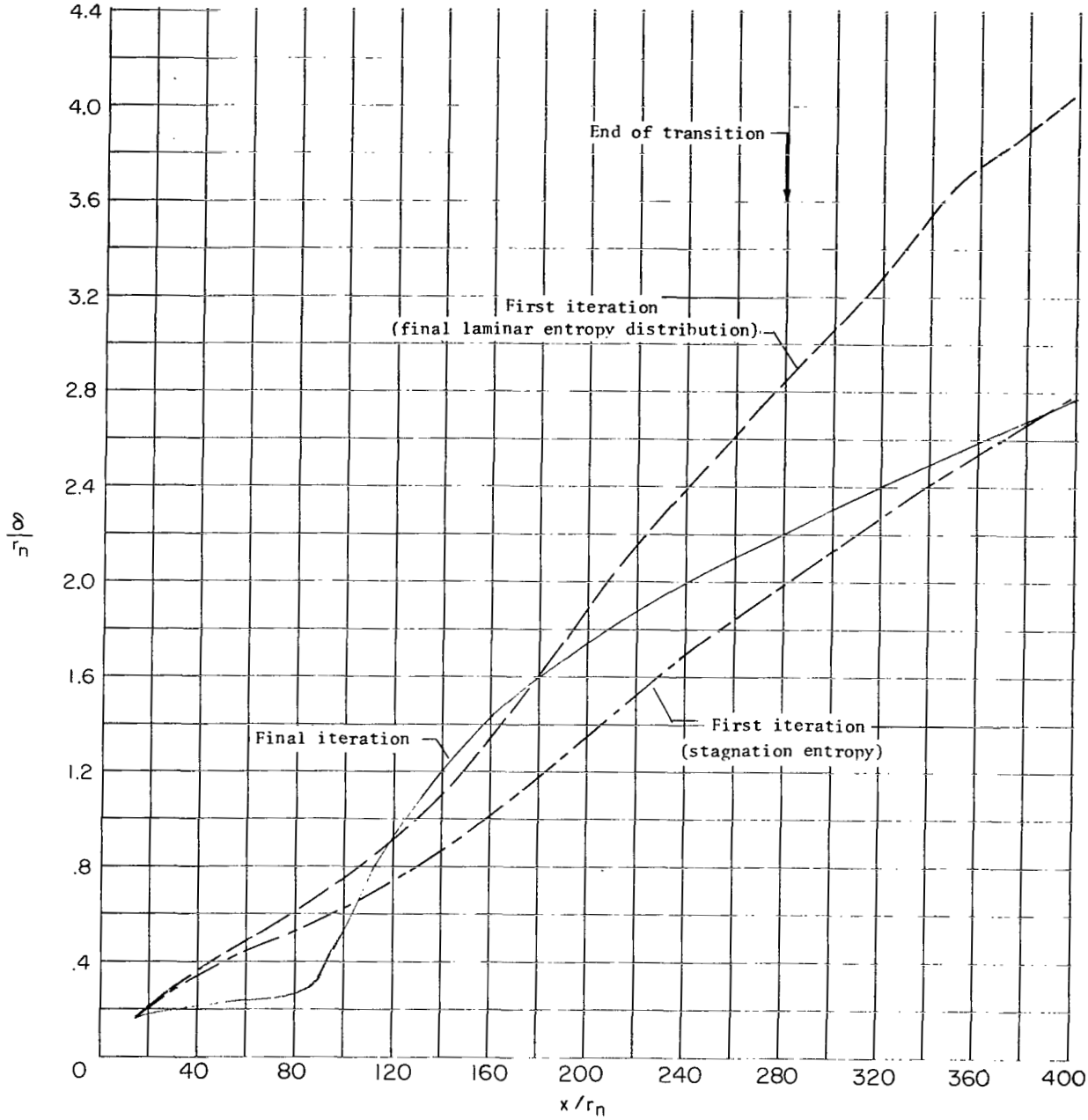

Figure 10.- The effect of three entropy distributions at the edge of the boundary layer on boundary-layer thickness for three turbulent-boundary-layer calculations at 18.29 km (60 000 ft) and u_∞ = 5.80 km/sec (19 019 ft/sec). r_n = 1.016 cm (0.4 in.).

edge condition. The u_e/u_∞ ratio at the end of the cone for the final turbulent calculation is approximately 1.35 times greater than the u_e/u_∞ ratio calculated from stagnation-entropy edge conditions. The h_e/H_e and u_e/u_∞ ratios from the final calculation for the turbulent boundary layer approach the sharp-cone values at approximately an x/r_n of ~~200~~ 100. The values of h_e/H_e, ρ_e, T_e, M_e, and u_e are shown in table III, at

TABLE III.- THE VALUES OF VELOCITY, DENSITY, TEMPERATURE, AND MACH NUMBER AT $\frac{x}{r_n} = 400$ FOR STAGNATION AND VARIABLE ENTROPY CONDITIONS

[Altitude, 18.29 km (60 000 ft); V_∞ = 5.80 km/sec (19 019 ft/sec)]

	Stagnation entropy	Final turbulent calculation
h_e/H_e	0.4655	0.02133
ρ_e, kg/m^3 (lbm/cu ft)	0.0314 (0.00195)	0.4019 (0.02509)
T_e, K ($^\circ$R)	3960 (7128)	358.7 (645.6)
M_e	3.34	15.15
u_e, km/sec (ft/sec)	4.264 (13 990)	5.77 (18 930)

$\frac{x}{r_n} = 400$, for an entropy distribution change from a stagnation value to the final turbulent value. The flow properties of h_e/H_e, ρ_e, T_e, M_e, and u_e vary by factors of 21.8, 12.9, 11.0, 4.5, and 1.4 respectively. Thus, for the same change in entropy distribution, the variation of flow properties can be as small as a factor of 1.4 (u_e) and as large as a factor of 21.8 (h_e/H_e).

Boundary-layer parameters.- The boundary-layer parameters $(N, \theta/r_n, \delta/r_n,$ and $\delta^*/r_n)$ shown in figures 8 to 11 were calculated from the same boundary-layer calculation used to determine the edge properties shown in figures 5 to 7. The variation of the N "power-law" exponent for the three sets of conditions at the edge of the boundary layer is shown in figure 8. The value of N at the end of the cone $\left(\frac{x}{r_n} = 400\right)$ varies from approximately 4.3 for the edge conditions based on stagnation entropy to a value of approximately 9.8 for the final calculation for a turbulent boundary layer. The calculations for all three entropy distributions start at the beginning of transition with N = 1.5 based on a laminar boundary-layer profile.

The dimensionless momentum thickness θ/r_n shown in figure 9 for the three edge condition distributions is calculated from an integration of equation (3). The decrease in θ/r_n from the start of the final iteration to an x/r_n of approximately 100 would imply a negative skin friction, that is, for sharp-cone conditions where $\frac{d\theta/r_n}{dx/r_n}$ is equal to $C_f/2$. However, the reason for a decrease in θ/r_n is not from a negative value in $C_f/2$ but from the combined effects of variable entropy and transitional flow which is felt in equation (3) in terms of: (1) the value of the edge condition gradients; (2) the variable-entropy term (eq. (6)); (3) the value of $(\delta^*/r_n)/(\theta/r_n)$ term; and (4) the value of $C_f/2$. Thus, the combination of these effects has a significant effect on the integration of the momentum equation and the resulting value of θ/r_n.

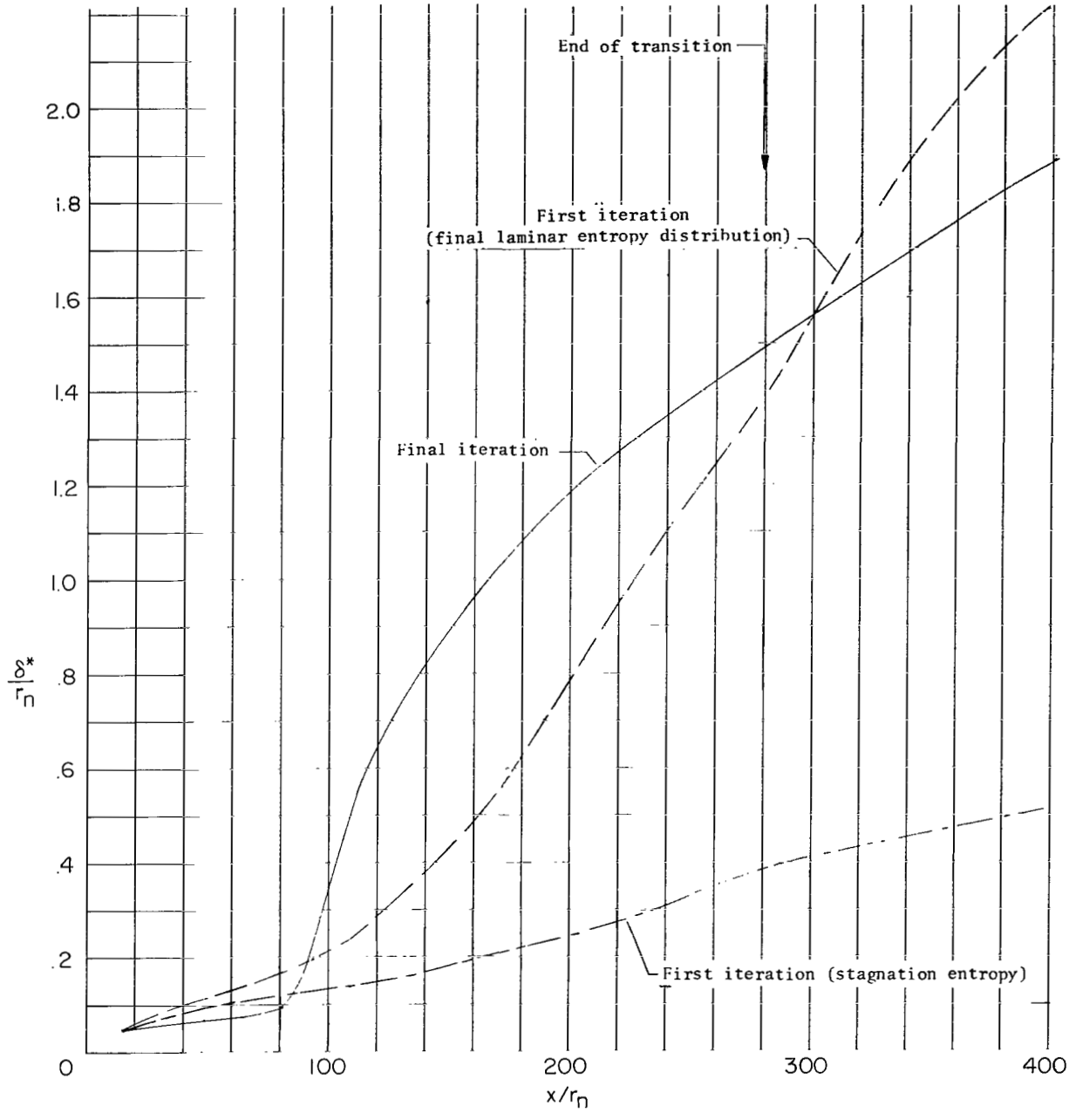

Figure 11.- The effect of three entropy distributions at the edge of the boundary layer on the displacement thickness for three turbulent-boundary-layer calculations at 18.29 km (60 000 ft) and u_∞ = 5.80 km/sec (19 019 ft/sec). r_n = 1.016 cm (0.4 in.).

The effect of three different edge conditions on the calculation of the boundary-layer thickness δ/r_n and the displacement thickness δ^*/r_n is shown in figures 10 and 11. These results show no common trend in the growth of δ/r_n and δ^*/r_n with respect to the variation of the three edge (entropy) conditions. However, it appears because of the rapidly changing edge conditions, resulting from a change in local entropy from a

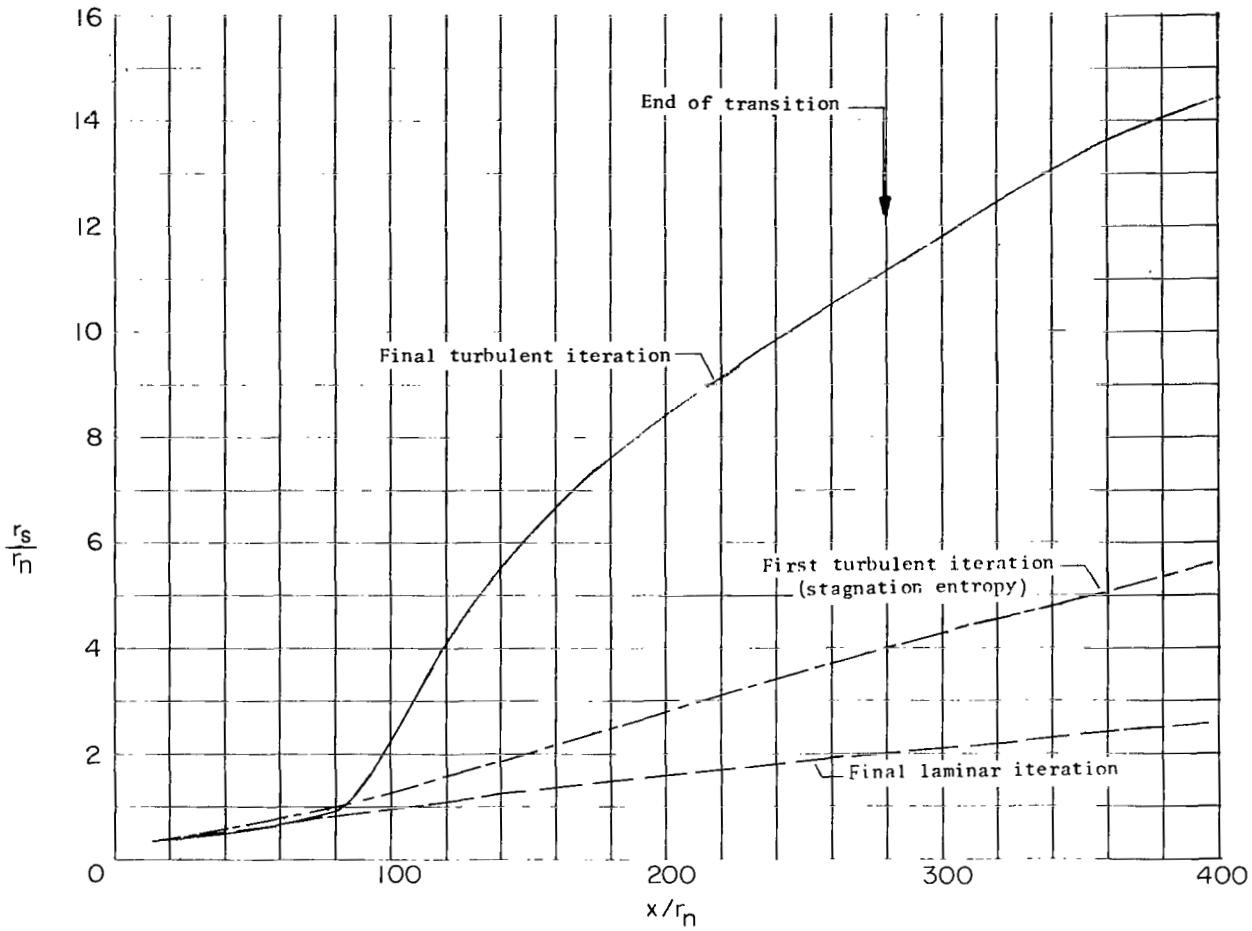

Figure 12.- The shock radius distribution based on a mass rate of flow into the boundary layer for two turbulent- and one laminar-boundary-layer calculations at 18.29 km (60 000 ft) and u_∞ = 5.80 km/sec (19 019 ft/sec). r_n = 1.016 cm (0.4 in.).

stagnation to a sharp-cone value, that δ/r_n and δ^*/r_n may not follow the classical variation with $R_{e,x}$ $\left(\text{that is, } \frac{\delta^*}{x} \propto \frac{1}{R_{e,x}^{1/5}} \text{ and } \frac{\delta}{x} \propto \frac{1}{R_{e,x}^{1/5}}\right)$, but are strongly Mach number dependent, the value of δ/r_n and δ^*/r_n increasing with increasing Mach number.

The shock radius r_s/r_n (see eq. (19)) shown in figure 12 is used to determine the value of entropy at the edge of the boundary layer. The values of r_s/r_n in figure 12 labeled "Final laminar iteration" were calculated during the final iterative solution for laminar flow (ref. 33) and were used to determine the entropy distribution for the first iteration in the solution for turbulent flow. The r_s/r_n values calculated for the turbulent boundary layer from stagnation entropy distributions are greater than the values calculated from the final iteration for a laminar boundary layer; this result indicates that even for a low Mach number (that is, $M_e \approx 3.5$), the turbulent boundary layer has a larger

mass entrainment than the laminar boundary layer. It can be seen from figure 12 that the mass entrainment for the final calculation of the turbulent boundary layer is very large compared with the calculation of mass entrainment for either the laminar boundary layer or the turbulent boundary layer with stagnation conditions at the edge of the boundary layer.

Skin friction.- The local skin friction $C_f/2$ used in the calculations for figures 5 to 12 is shown in figure 13. The skin friction is calculated from the Van Driest II (ref. 39) theory. (See table II.) The initial value of $C_f/2$ at the start of transition is taken from the solution for laminar flow $\left(\text{that is, } \frac{C_f}{2} = 1.02 \times 10^{-3}\right)$. For the two "first iteration" calculations, equation (25) cannot be used and, as a result, the value of $C_f/2$ jumps from the initial laminar value to the value calculated by the Van Driest II (ref. 6) theory. The level of $C_f/2$ in figure 13 decreases as the entropy distribution changes from (1) stagnation, (2) to laminar calculation, and (3) to a final iteration value. In terms of the classical variation of $C_f/2$ with $R_{e,x}$, the decrease in $C_f/2$ for the final iteration calculation would be expected, based on the corresponding rapid increase in the value of $R_{e,x}$ shown in figure 6. However, the variation of $C_f/2$ for the final calculation is more complex, in terms of shear and heat transfer, than would appear from the results in figure 13.

The variation of the wall shear calculated from

$$\tau_w = \frac{C_f}{2} \rho_e u_e^2 \tag{30}$$

is shown in figure 14 for three entropy distributions. The shear for the final calculation for turbulent flow shows a rapid rise at the start of transition to a nearly constant value for the fully turbulent flow. However, the rapid rise in the transition region is not reflected in the corresponding value of $C_f/2$ in figure 13. The reason for the rapid rise in shear can be seen by examining the variation of $\rho_e u_e^2$ (fig. 15) through the transition region as calculated for the same edge conditions used in figures 13 and 14. A comparison of the final iteration results in figures 14 and 15 from the beginning to the end of transition region shows that $\rho_e u_e^2$ increases by a factor of approximately 25 whereas τ_w only increases by a factor of 5. These increases result in a factor of 5 decrease in $C_f/2$ in the transition region. It should be noted that the heat transfer in the transition region is similarly affected by a rapid rise in the product of $\rho_e u_e$. The rise in $\rho_e u_e$ when coupled with a nearly constant value in $h_{aw} - h_w$ produces a rapid rise in the heating rates in the transition region. (See eqs. (28) and (29).)

Effect of nose radius.- The effect of nose radius on the local Mach number and Reynolds number is shown in figures 16 and 17, respectively. The results shown in these two figures were taken from the final iteration of a variable-entropy calculation for turbulent flow at zero angle of attack, at an altitude of 18.29 km (60 000 ft), and a velocity of

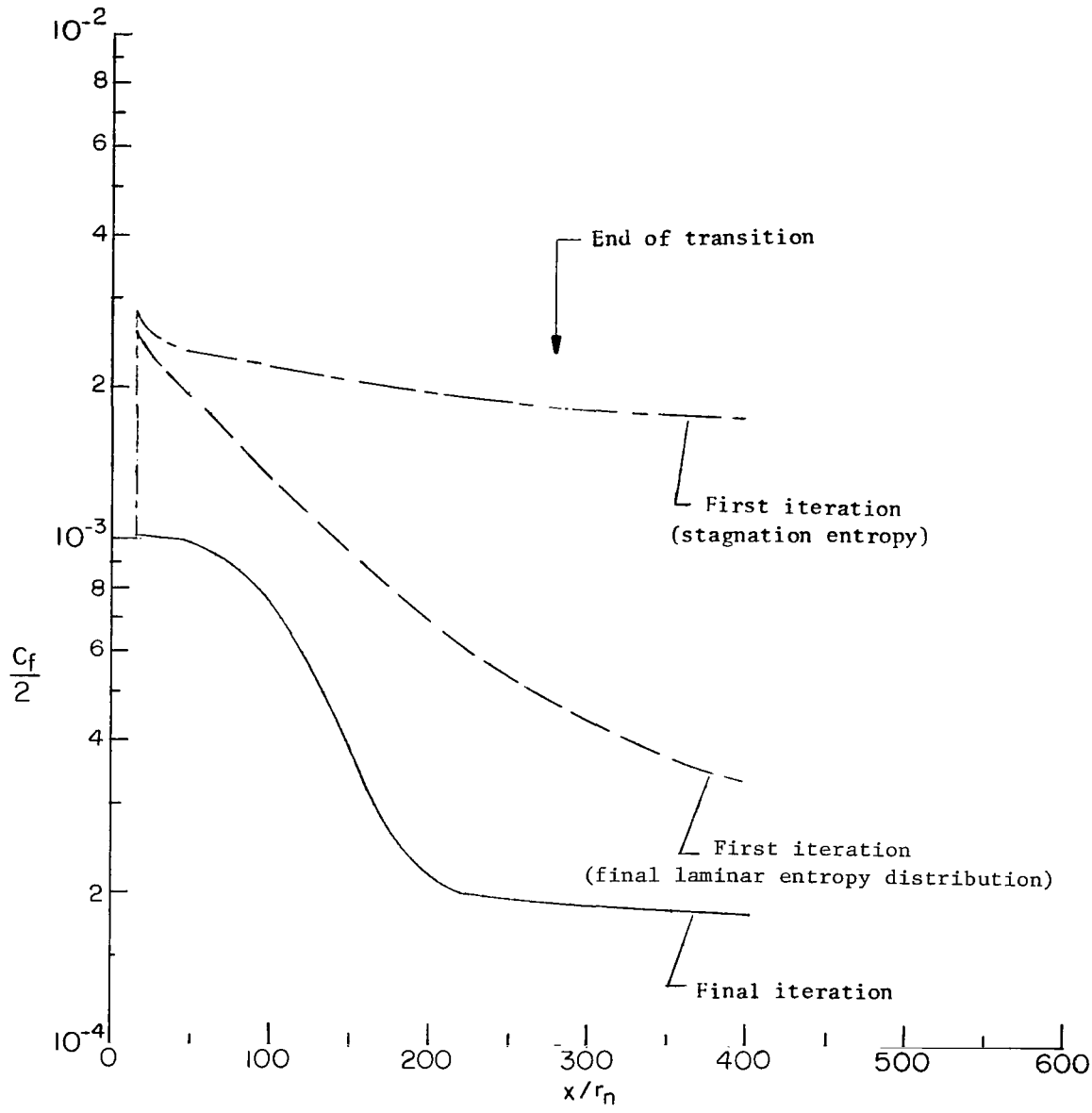

Figure 13.- The effect of three entropy distributions at the edge of the boundary layer on the local skin-friction coefficient for three turbulent-boundary-layer calculations at 18.29 km (60 000 ft) and u_∞ = 5.80 km/sec (19 019 ft/sec). r_n = 1.016 cm (0.4 in.).

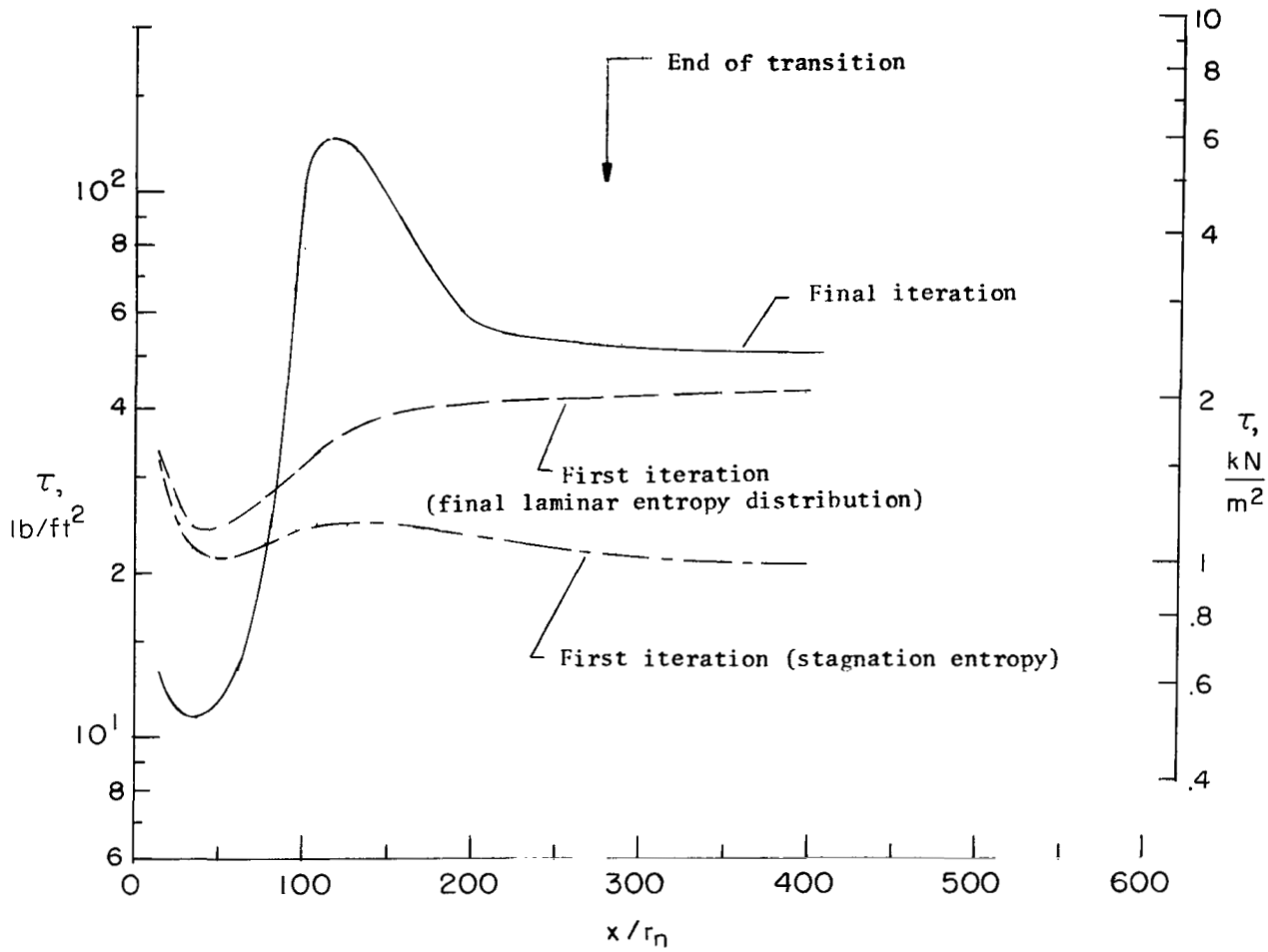

Figure 14.- The effect of three entropy distributions at the edge of the boundary layer on the shear stress at the wall for three turbulent-boundary-layer calculations at 18.29 km (60 000 ft) and u_∞ = 5.80 km/sec (19 019 ft/sec). r_n = 1.016 cm (0.4 in.).

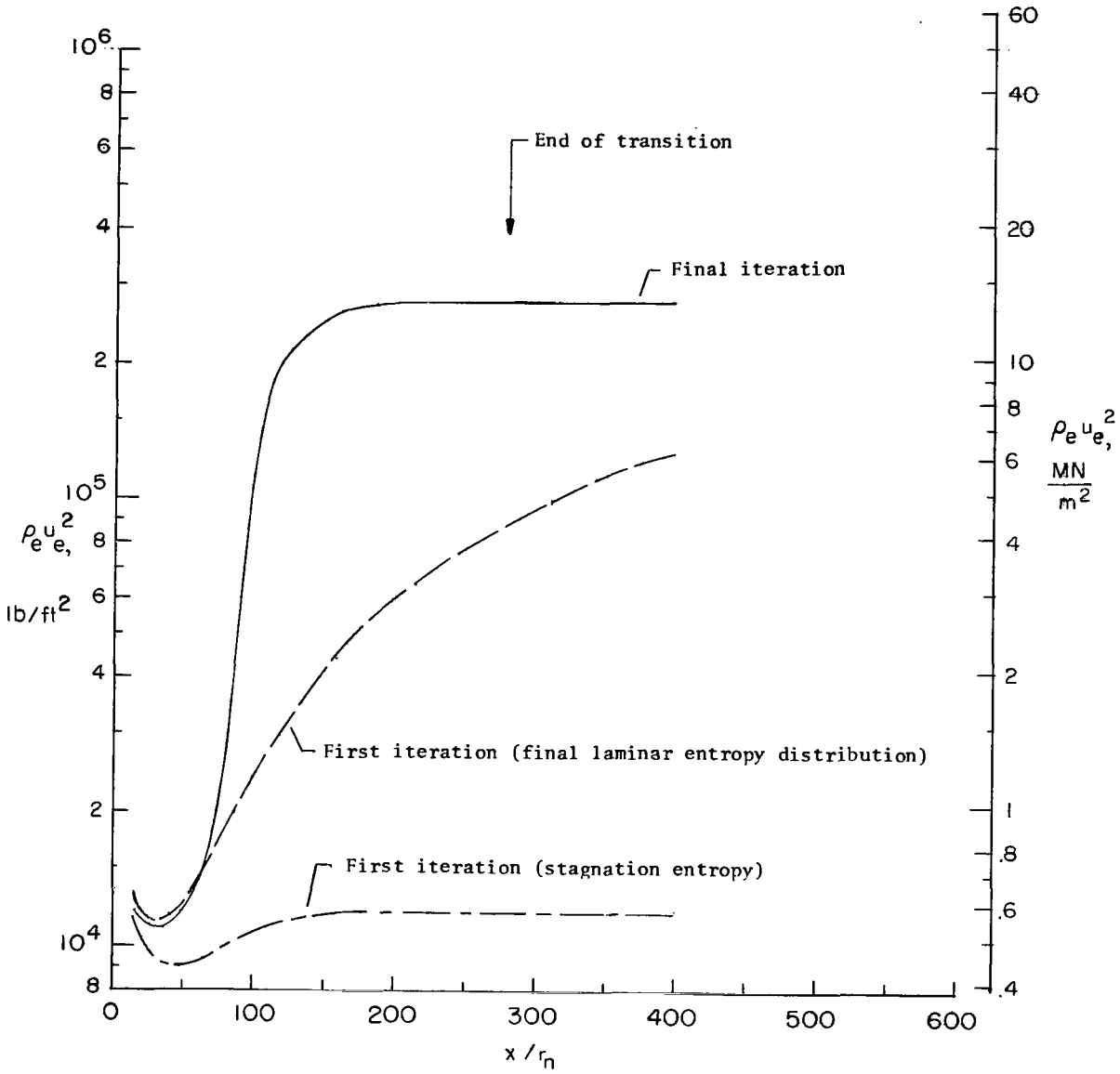

Figure 15.- The effect of three entropy distributions at the edge of the boundary layer on the local value of $\rho_e u_e^2$ for three turbulent-boundary-layer calculations at 18.29 km (60 000 ft) and u_∞ = 5.80 km/sec (19 019 ft/sec). r_n = 1.016 cm (0.4 in.).

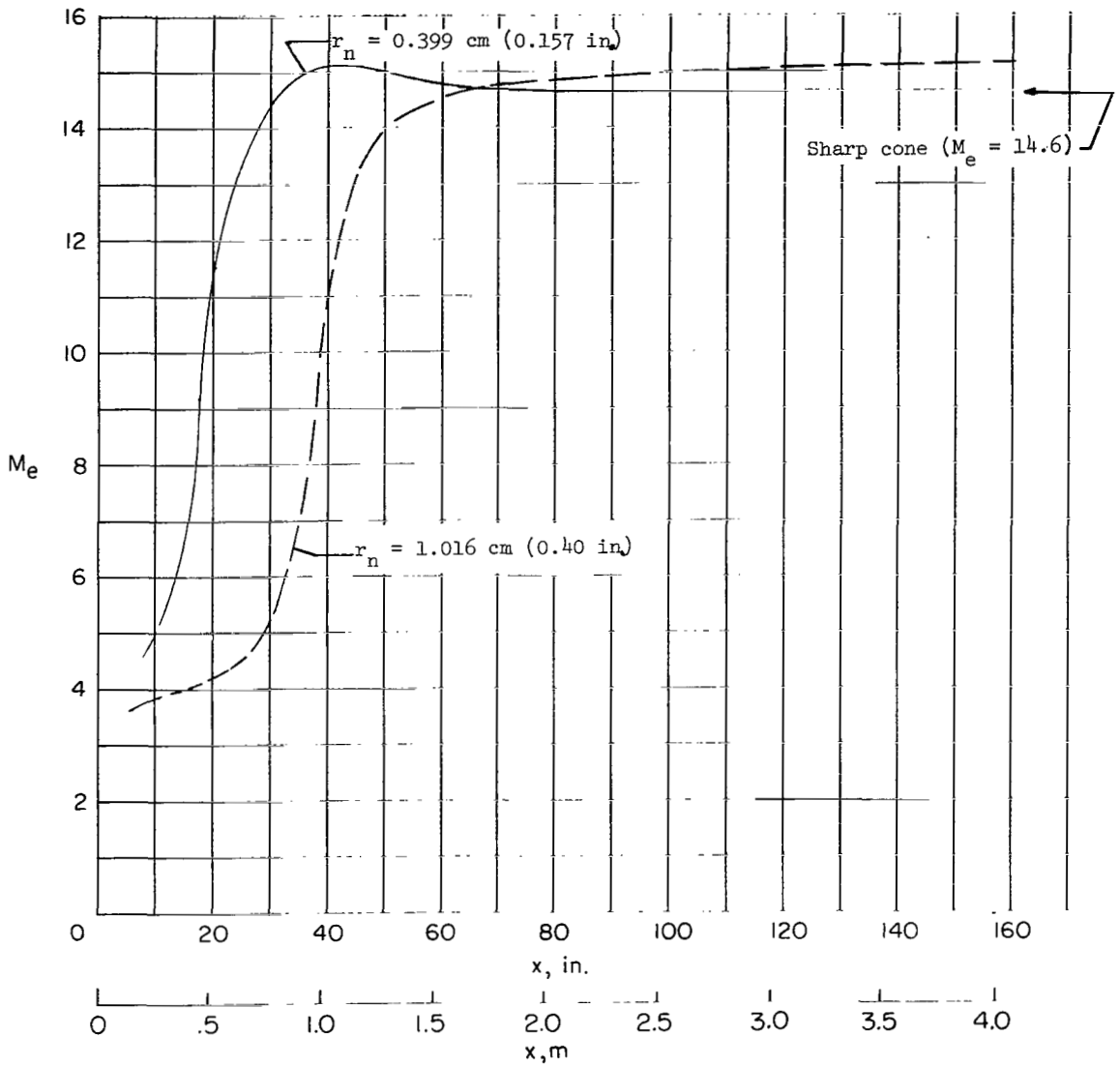

Figure 16.- The effect of nose bluntness on the local Mach number for the final iteration calculation on the turbulent boundary layer at 18.29 km (60 000 ft) and u_∞ = 5.80 km/sec (19 019 ft/sec).

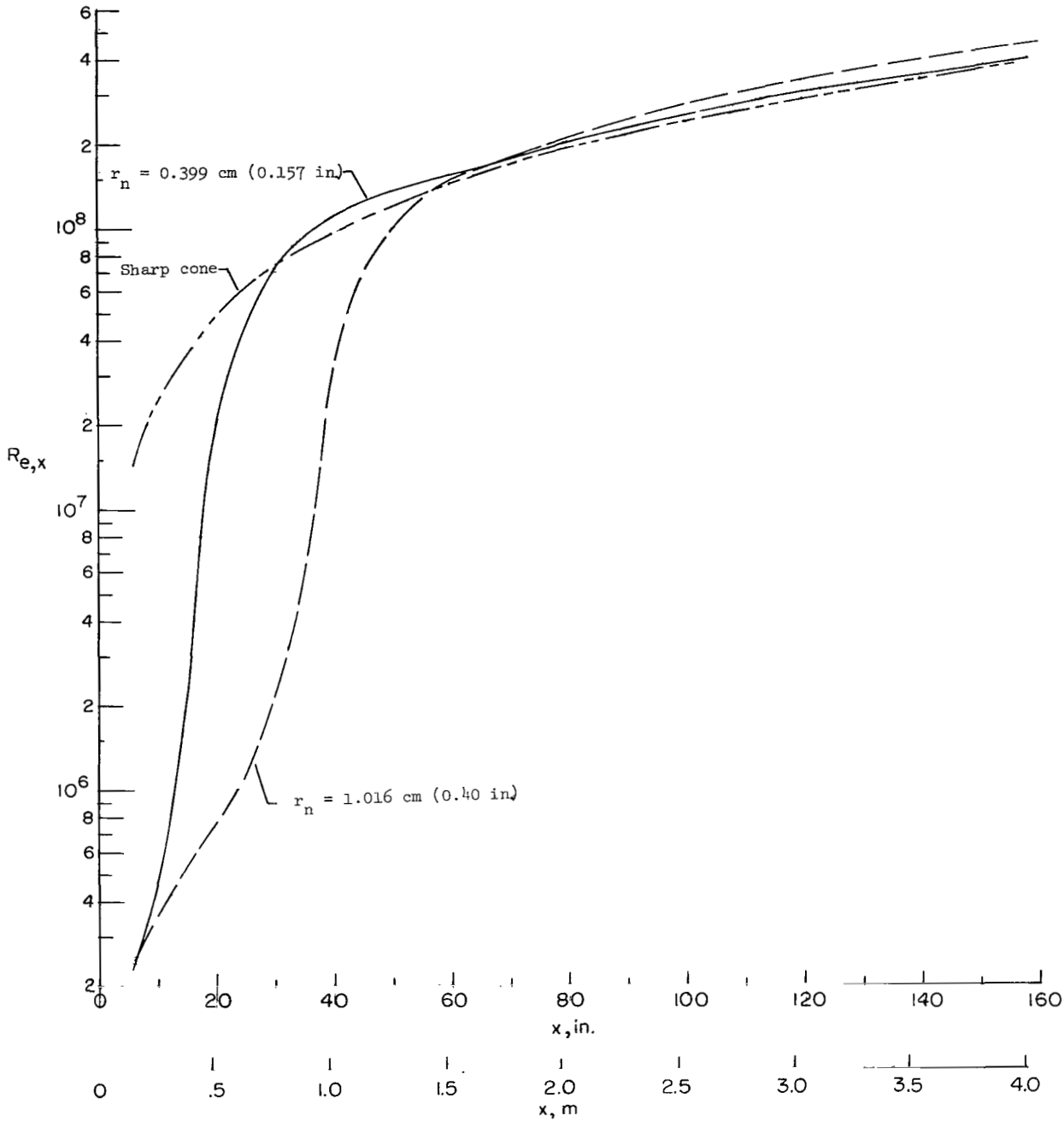

Figure 17.- The effect of nose bluntness on the local Reynolds number for the final iteration calculations on the turbulent boundary layer at 18.29 km (60 000 ft) and u_∞ = 5.80 km/sec (19 019 ft/sec).

5.80 km/sec (19 019 ft/sec) for nose radii of 1.016 cm (0.4 in.) and 0.399 cm (0.157 in.). The start of transition was again assumed to be at $x = 15.24$ cm (6.0 in.), and the end of transition was assumed to be at 2.26 m (89.0 in.) for both nose radii. The results in figures 16 and 17 show that the smaller nose radius $\left(r_n = 0.399 \text{ cm } (0.157 \text{ in.})\right)$ approaches a sharp-cone value of Mach number and Reynolds number faster than the large nose radius $\left(r_n = 1.016 \text{ cm } (0.40 \text{ in.})\right)$. For both nose radii the local Mach number and local Reynolds number overshoot the sharp-cone values. However, at the end of the cone that has a 0.399 cm (0.157-in.) nose radius, the values of $R_{e,x}$ and M_e have become asymptotic to the sharp-cone values.

CONCLUDING REMARKS

A simple integral technique for calculating the transitional and turbulent boundary layers for equilibrium air on an axisymmetric body at zero angle of attack – including the effects of variable entropy – has been presented. Boundary-layer velocity profiles were calculated from an N power-law correlation. Density profiles were calculated by use of a modified Crocco relationship. Skin friction was determined from either the Van Driest II or Spalding-Chi theories, by use of a momentum thickness Reynolds number. Heat transfer was calculated by using a modified form of Reynolds analogy. The Reynolds analogy factor, used with the Van Driest II skin-friction theory, varied as a function of wall enthalpy ratio h_w/H_e from 1.0 to 1.2, but with the Spalding-Chi theory it was held constant at $\left(N'_{Pr}\right)^{-2/3}$.

Calculations of heat transfer for transitional and turbulent flow agreed with data measured on a flat plate at Mach 6.0 and two blunt cones at Mach 8.0 and 11.5. The calculations for the flat plate showed that the transformation function F_c used to transform the skin friction to the compressible plane must be calculated with the assumption of a linear Crocco relationship. The predictions of heat transfer on the flat plate obtained by use of the integral theory are in agreement with a finite-difference theory. Both the Van Driest II and Spalding-Chi skin-friction theories gave a reasonable prediction of heat transfer for the Mach 8.0 cone data provided the proper Reynolds analogy factor was used.

Sample turbulent-boundary-layer flight calculations were made at an altitude of 18.29 km (60 000 ft) and flight conditions of approximately 6.09 km/sec (20 000 ft/sec) for a 3.96-meter-long (13-ft), 5° half-angle cone with a nose radius of 1.016 cm (0.40 in.). The calculations were made for three entropy distributions: (1) stagnation value; (2) laminar-boundary-layer values; and (3) turbulent-boundary-layer values. The calculation showed that mass entrainment was considerably larger for the turbulent-boundary-layer distribution than for the other two distributions; as a result, a sharp-cone entropy was reached at approximately ~~250~~ 165 nose radii from the nose of the cone. The calculation

showed that as the edge entropy decreased, the shear at the wall increased considerably, whereas at the same time the skin-friction coefficient showed a marked decrease.

Langley Research Center,
National Aeronautics and Space Administration,
Hampton, Va., April 6, 1971.

APPENDIX

TRANSFORMATION OF THE LOCAL AND AVERAGE TURBULENT SKIN FRICTION FROM A FLAT-PLATE TO A SHARP-CONE VALUE

Local Skin Friction

The general form of the Mangler transformation factor F_{MT} (see ref. 41) converting local flat-plate skin friction to a sharp-cone value is

$$F_{MT} = \frac{C_f\big|_{Cone}}{C_f\big|_{Flat\ plate}} = \left[\frac{\frac{x}{r_n}\left(\frac{r_b}{r_n}\right)^{\frac{n}{n-1}}}{\int_0^{x/r_n}\left(\frac{r_b}{r_n}\right)^{\frac{n}{n-1}} d\,\frac{x}{r_n}}\right]^{1/n} \tag{31}$$

When the Blasius form of the turbulent skin friction for a flat plate

$$C_f \propto R_{e,x}^{-1/n} \tag{32}$$

is used, with $n = 5.0$, along with the assumption of turbulent flow over the entire cone, the resulting Mangler transformation factor is

$$F_{MT} = 1.176 \tag{33}$$

In the region of fully turbulent flow, the $F_{MT} = 1.176$ (eq. (33)) was used for the calculations in which the Van Driest II skin-friction theory was used. When the Spalding-Chi skin-friction theory was used, an alternate variation of the F_{MT} was used which took into account the transition from a laminar F_{MT} $(\sqrt{3})$ to a turbulent F_{MT} (1.176) in the form

$$F_{MT}^2 - 2\sqrt{3}\,F_{MT} + 3.0 = \overline{P}\left[\frac{x}{r_n} - \left(\frac{x_{vo}}{r_n}\right)_o\right] \tag{34}$$

where

$$\overline{P} = \frac{0.309136}{\left[\left(\frac{x}{r_n}\right)_{max} - \left(\frac{x_{vo}}{r_n}\right)_o\right]}$$

The $(x_{vo}/r_n)_o$ term was evaluated at the beginning of fully turbulent flow from equation (9) and the $(x/r_n)_{max}$ was evaluated at the end of the cone.

A check was made on the effect of nose bluntness on the value of F_{MT} found from equation (31) for a 3.96-meter-long (13-ft), 5^o half-angle cone with a 1.016-cm (0.4-in.)

nose radius. The check showed that the value of F_{MT} which included the effects of nose bluntness was less than 1.0 percent smaller than the value of 1.176 (eq. (33)) found for a sharp cone.

Average Skin Friction

The ratio of the average skin friction on a sharp cone to that on a flat plate is

$$\frac{\overline{C}_F\Big|_{Cone}}{\overline{C}_F\Big|_{Flat\ plate}} = \frac{\dfrac{\int_0^L (C_f)_{Cone}\, dA}{\int_0^L dA}}{\dfrac{\int_0^L (C_f)_{Flat\ plate}\, d\frac{x}{r_n}}{\int_0^L d\frac{x}{r_n}}} \tag{35}$$

where L is a constant and is the same for the flat plate and cone. When equations (32) and (33) are substituted into equation (35) and the indicated integration is performed, the resulting ratio of the average skin friction on a cone to that on a flat plate is

$$\frac{\overline{C}_F\Big|_{Cone}}{\overline{C}_F\Big|_{Flat\ plate}} = 1.045 \tag{36}$$

REFERENCES

1. Bradshaw, P.: Boundary-Layer Problems of 1967. NPL Aero Rep. 1253, Brit. A.R.C., Sept. 1967.

2. Rotta, J. C.: Recent Developments in Calculation Methods for Turbulent Boundary Layers With Pressure Gradients and Heat Transfer. Trans. ASME, Ser. E.: J. Appl. Mech., vol. 33, no. 2, June 1966, pp. 429-437.

3. Hornung, H. G.: A Survey of Compressible Flow Boundary Layers – Theory and Experiment. Rep. ACA 67, Dep. Supply, Australian Aeronaut. Res. Comm., Feb. 1966.

4. Beckwith, Ivan E.: Recent Advances in Research on Compressible Turbulent Boundary Layers. Analytic Methods in Aircraft Aerodynamics, NASA SP-228, 1970, pp. 355-416.

5. McDonald, Henry: An Assessment of Certain Procedures for Computing the Compressible Turbulent Boundary Layer Development. Compressible Turbulent Boundary Layers, NASA SP-216, 1968, pp. 181-229.

6. Hopkins, Edward J.; Keener, Earl R.; and Louie, Pearl T.: Direct Measurements of Turbulent Skin Friction on a Nonadiabatic Flat Plate at Mach Number 6.5 and Comparisons with Eight Theories. NASA TN D-5675, 1970.

7. Spalding, D. B.; and Chi, S. W.: The Drag of a Compressible Turbulent Boundary Layer on a Smooth Flat Plate With and Without Heat Transfer. J. Fluid Mech., vol. 18, pt. 1, Jan. 1964, pp. 117-143.

8. Bushnell, Dennis M.; Johnson, Charles B.; Harvey, William D.; and Feller, William V.: Comparison of Prediction Methods and Studies of Relaxation in Hypersonic Turbulent Nozzle-Wall Boundary Layers. NASA TN D-5433, 1969.

9. Johnson, Charles B.; Boney, Lillian R.; Ellison, James C.; and Erickson, Wayne D.: Real-Gas Effects on Hypersonic Nozzle Contours With a Method of Calculation. NASA TN D-1622, 1963.

10. Fluid Motion Sub-Committee of the Aeronautical Research Council: Modern Developments in Fluid Dynamics. High Speed Flow. Vol. II, L. Howarth, ed., Clarendon Press (Oxford), 1953.

11. Shutts, W. H.; Hartwig, W. H.; and Weiler, J. E.: Final Report on Turbulent Boundary-Layer and Skin-Friction Measurements on a Smooth, Thermally Insulated Flat Plate at Supersonic Speeds. DRL-364, CM-823 (Contract NOrd-9195), Univ. of Texas, Jan. 5, 1955.

12. Coles, Donald: Measurements in the Boundary Layer on a Smooth Flat Plate in Supersonic Flow. III. Measurements in a Flat-Plate Boundary Layer at the Jet Propulsion Laboratory. Report No. 20-71 (Contract No. DA-04-495-Ord 18), Jet Propulsion Lab., California Inst. Technol., June 1, 1953.

13. Danberg, James E.: Measurement of the Characteristics of the Compressible Turbulent Boundary Layer With Air Injection. NAVORD Rep. 6683, U.S. Navy, Sept. 3, 1959.

14. Danberg, James E.: Characteristics of the Turbulent Boundary Layer With Heat and Mass Transfer: Data Tabulation. NOLTR 67-6, U.S. Navy, Jan. 23, 1967. (Available from DDC as AD 650 272.)

15. Danberg, James E.: Characteristics of the Turbulent Boundary Layer With Heat and Mass Transfer at $M = 6.7$. NOLTR 64-99, U.S. Navy, Oct. 19, 1964. (Available from DDC as AD 452 471.)

16. Winkler, Eva M., and Cha, Moon H.: Investigation of Flat Plate Hypersonic Turbulent Boundary Layers With Heat Transfer at a Mach Number of 5.2. NAVORD Rep. 6631, U.S. Navy, Sept. 15, 1959.

17. Gooderum, Paul B.: An Experimental Study of the Turbulent Boundary Layer on a Shock-Tube Wall. NACA TN 4243, 1958.

18. Adcock, Jerry B.; Peterson, John B., Jr.; and McRee, Donald I.: Experimental Investigation of a Turbulent Boundary Layer at Mach 6, High Reynolds Numbers, and Zero Heat Transfer. NASA TN D-2907, 1965.

19. Allen, Jerry M.; and Monta, William J.: Turbulent-Boundary-Layer Characteristics of Pointed Slender Bodies of Revolution at Supersonic Speeds. NASA TN D-4193, 1967.

20. Monaghan, R. J.; and Cooke, J. R.: The Measurement of Heat Transfer and Skin Friction at Supersonic Speeds. Part IV – Tests on a Flat Plate at $M = 2.82$. C.P. No. 140, British A.R.C., 1953.

21. Pinckney, S. Z.: Data on Effects of Incident-Reflecting Shocks on the Turbulent Boundary Layer. NASA TM X-1221, 1966.

22. Wilson, R. E.: Characteristics of Turbulent Boundary Layer Flow Over a Smooth, Thermally Insulated Flat Plate at Supersonic Speeds. DRL 301, CM-712 (Contract NOrd-9195), Univ. of Texas, June 1, 1952.

23. Maddalon, Dal V.; and Henderson, Arthur, Jr.: Boundary Layer Transition on Sharp Cones at Hypersonic Mach Numbers. AIAA J., vol. 6, no. 3, Mar. 1968, pp. 424-431.

24. Henderson, A.; Rogallo, R. S.; Woods, W. C.; and Spitzer, C. R.: Exploratory Hypersonic Boundary-Layer Transition Studies. AIAA J., vol. 3, no. 7, July 1965, pp. 1363-1364.

25. Scaggs, Norman E.: Boundary Layer Profile Measurements in Hypersonic Nozzles. ARL 66-0141, U.S. Air Force, July 1966.

26. Johnson, Charles B.; and Bushnell, Dennis M.: Power-Law Velocity-Profile Exponent Variations With Reynolds Number, Wall Cooling, and Mach Number in a Turbulent Boundary Layer. NASA TN D-5753, 1970.

27. Lomax, Harvard; and Inouye, Mamoru: Numerical Analysis of Flow Properties About Blunt Bodies Moving at Supersonic Speeds in An Equilibrium Gas. NASA TR R-204, 1964.

28. Eckert, E. R. G.: Engineering Relations for Heat Transfer and Friction in High-Velocity Laminar and Turbulent Boundary-Layer Flow Over Surfaces With Constant Pressure and Temperature. Trans. ASME, vol. 78, no. 6, Aug. 1956, pp. 1273-1283.

29. Hansen, C. Frederick: Approximations for the Thermodynamic and Transport Properties of High-Temperature Air. NASA TR R-50, 1959. (Supersedes NACA TN 4150.)

30. Hopkins, Edward J.; Rubesin, Morris W.; Inouye, Mamoru; Keener, Earl R.; Mateer, George C.; and Polek, Thomas E.: Summary and Correlation of Skin-Friction and Heat-Transfer Data for a Hypersonic Turbulent Boundary Layer on Simple Shapes. NASA TN D-5089, 1969.

31. Van Driest, E. R.: The Problem of Aerodynamic Heating. Aeronaut. Eng. Rev., vol. 15, no. 10, Oct. 1956, pp. 26-41.

32. Cary, Aubrey M., Jr.: Summary of Available Information on Reynolds Analogy for Zero-Pressure-Gradient Compressible, Turbulent-Boundary-Layer Flow. NASA TN D-5560, 1970.

33. Wilson, Donald M.: A Correlation of Heat-Transfer and Skin-Friction Data and an Experimental Reynolds Analogy Factor for Highly Cooled Turbulent Boundary Layers at Mach 5.0. NOLTR-69-51, U.S. Navy, Mar. 5, 1969. (Available from DDC as AD 690 454.)

34. Inouye, Mamoru; Rakich, John V.; and Lomax, Harvard: A Description of Numerical Methods and Computer Programs for Two-Dimensional and Axisymmetric Supersonic Flow Over Blunt-Nosed and Flared Bodies. NASA TN D-2970, 1965.

35. Stainback, P. Calvin (With appendix by P. Calvin Stainback and Kathleen C. Wicker): Effect of Unit Reynolds Number, Nose Bluntness, Angle of Attack, and Roughness on Transition on a 5^{o} Half-Angle Cone at Mach 8. NASA TN D-4961, 1969.

36. Potter, J. Leith; and Whitfield, Jack D.: Effects of Slight Nose Bluntness and Roughness on Boundary-Layer Transition in Supersonic Flows. J. Fluid Mech., vol. 12, pt. 4, Apr. 1962, pp. 501-535.

37. Cary, Aubrey M., Jr.: Turbulent-Boundary-Layer Heat-Transfer and Transition Measurements With Surface Cooling at Mach 6. NASA TN D-5863, 1970.

38. Harris, Julius Elmore: Numerical Solution of the Compressible Laminar, Transitional, and Turbulent Boundary Layer Equations With Comparisons to Experimental Data. Ph. D. Thesis, Virginia Polytech. Inst., May 1970.

39. Softley, E. J.; Graber, B. C.; and Zempel, R. E.: Experimental Observation of Transition of the Hypersonic Boundary Layer. AIAA J., vol. 7, no. 2, Feb. 1969, pp. 257-263.

40. Stainback, P. Calvin: Heat-Transfer Measurements at a Mach Number of 4.95 on Two 60° Swept Delta Wings With Blunt Leading Edges and Dihedral Angles of 0° and 45°. NASA TN D-549, 1961.

41. Bertram, Mitchel H.; and Neal, Luther, Jr.: Recent Experiments in Hypersonic Turbulent Boundary Layers. Presented at the AGARD Specialist's Meeting on Recent Developments in Boundary-Layer Research (Naples, Italy), May 10-14, 1965.

NASA-Langley, 1971 — 12 L-7415

02U 001 37 51 3DS 71166 00903
AIR FORCE WEAPONS LABORATORY /WLOL/
KIRTLAND AFB, NEW MEXICO 87117

ATT E. LOU BOWMAN, CHIEF,TECH. LIBRARY

"The aeronautical and space activities of the United States shall be conducted so as to contribute . . . to the expansion of human knowledge of phenomena in the atmosphere and space. The Administration shall provide for the widest practicable and appropriate dissemination of information concerning its activities and the results thereof."

— NATIONAL AERONAUTICS AND SPACE ACT OF 1958

NASA SCIENTIFIC AND TECHNICAL PUBLICATIONS

TECHNICAL REPORTS: Scientific and technical information considered important, complete, and a lasting contribution to existing knowledge.

TECHNICAL NOTES: Information less broad in scope but nevertheless of importance as a contribution to existing knowledge.

TECHNICAL MEMORANDUMS: Information receiving limited distribution because of preliminary data, security classification, or other reasons.

CONTRACTOR REPORTS: Scientific and technical information generated under a NASA contract or grant and considered an important contribution to existing knowledge.

TECHNICAL TRANSLATIONS: Information published in a foreign language considered to merit NASA distribution in English.

SPECIAL PUBLICATIONS: Information derived from or of value to NASA activities. Publications include conference proceedings, monographs, data compilations, handbooks, sourcebooks, and special bibliographies.

TECHNOLOGY UTILIZATION PUBLICATIONS: Information on technology used by NASA that may be of particular interest in commercial and other non-aerospace applications. Publications include Tech Briefs, Technology Utilization Reports and Technology Surveys.

Details on the availability of these publications may be obtained from:

SCIENTIFIC AND TECHNICAL INFORMATION OFFICE

NATIONAL AERONAUTICS AND SPACE ADMINISTRATION

Washington, D.C. 20546